ALTEX Online first
published July 7, 2016
http://dx.doi.org/10.14573/altex.1605041

Research Article

3-D Nasal Cultures: Systems Toxicological Assessment of a Candidate Modified-Risk Tobacco Product

Anita R. Iskandar, Carole Mathis, Florian Martin, Patrice Leroy, Alain Sewer, Shoaib Majeed, Diana Kuehn, Keyur Trivedi, Davide Grandolfo, Maciej Cabanski, Emmanuel Guedj, Celine Merg, Stefan Frentzel, Nikolai V. Ivanov, Manuel C. Peitsch and Julia Hoeng
Philip Morris International R&D, Philip Morris Products S.A., Neuchâtel, Switzerland

Summary
In vitro toxicology approaches have evolved, from a focus on molecular changes within a cell to understanding of toxicity-related mechanisms in systems that can mimic the *in vivo* environment. The recent development of three dimensional (3-D) organotypic nasal epithelial culture models offers a physiologically robust system for studying the effects of exposure through inhalation. Exposure to cigarette smoke (CS) is associated with nasal inflammation; thus the nasal epithelium is relevant for evaluating the pathophysiological impact of CS exposure. The present study investigated further the application of *in vitro* human 3-D nasal epithelial culture models for toxicological assessment of inhalation exposure. Aligned with 3Rs strategy, this study aimed to explore the relevance of a human 3-D nasal culture model to assess the toxicological impact of aerosols generated from a candidate modified risk tobacco product (cMRTP), the Tobacco Heating System (THS) 2.2, as compared with smoke generated from reference cigarette 3R4F. A series of experimental repetitions where multiple concentrations of THS2.2 aerosol and 3R4F smoke were applied, were conducted to obtain reproducible measurements to understand the cellular/molecular changes that occur following exposure. In agreement with the Vision and Strategy of the Toxicity Testing in the 21st Century, this study implemented a systems toxicology approach and found that for all tested concentrations, the impact of 3R4F smoke was substantially greater than that of THS2.2 aerosol in terms of cytotoxicity levels, alterations in the tissue morphology, secretion of pro-inflammatory mediators, impaired ciliary function, and increased perturbed transcriptomes and miRNA expression profiles.

Keywords: air-liquid interface, organotypic culture, cigarette smoke, modified risk tobacco product, systems toxicology

1 Introduction[1]

Mechanistic investigation of the impact of exposure on the lower airway remains challenging because access to lung tissues is limited. Although biopsy samples can be obtained from patients/donors for mechanistic studies of exposure-induced injury, a biopsy procedure is invasive and there are related ethical concerns (Peppercorn, 2013). Alternatively, animal studies allow the collection of biological samples from various animal models of human diseases. However, biological responses can vary among animal species, and findings obtained from animal studies may not apply to humans. Alternatives to animal testing have been proposed to overcome these drawbacks, including the 3Rs strategy—reduction, refinement, and replacement of laboratory animals—to reduce the number of animals, to refine the design of procedures such that pain and distress are minimized, and to replace animal models with alternative methods and lower organisms when possible (Doke and Dhawale, 2015). In this regard, the capability to preserve human respiratory cells in culture provides a tool not only to generate mechanistic data, but also to improve the predicted effects of exposure hazard through inhalation in humans. An emphasis on assessment studies using human-derived *in vitro* culture systems will reduce the problems that are inherent to interspecies translatability (Manuppello and Sullivan, 2015).

[1]**Disclaimer**
All authors are employees of Philip Morris International. Philip Morris International is the sole source of funding and sponsor of this project.

Received May 4, 2016;
Accepted July 4, 2016;
Epub July 7, 2016;
http://dx.doi.org/10.14573/altex.1605041

This is an Open Access article distributed under the terms of the Creative Commons Attribution 4.0 International license (http://creativecommons.org/licenses/by/4.0/), which permits unrestricted use, distribution and reproduction in any medium, provided the original work is appropriately cited.

ALTEX Online first
published July 7, 2016
http://dx.doi.org/10.14573/altex.1605041

In vitro toxicology approaches have evolved from focusing on the molecular changes within a cell to understanding the toxicity-related mechanisms (cell–cell interactions) in models that closely mimic the *in vivo* environments. There are much efforts to reconstruct the *in vivo* tissue complexity using *in vitro* culture systems. Traditional submerged cultures exhibit a flat, squamous-like morphology and lack ciliated, secretory, and basal cells (Dimova et al., 2005). Recently developed three dimensional (3-D) human cell culture systems have allowed a better representation of the *in vivo* characteristics of the human respiratory tissue where the *in vivo*-like structure and function can be preserved.

The need for robust *in vitro* test systems of the nasal cavity has been driven mostly by the necessity to successfully deliver medications via the nasal route, such as the intranasal delivery of vaccines against respiratory infections (Kim, 2008). The nasal mucosa protect the sensitive lower airway tissues against harmful agents in the environment. Toxicant-induced injury in the nasal tissue can increase susceptibility to respiratory tract diseases (Harkema et al., 2006). The recent development of 3-D organotypic nasal epithelial cell culture models, including the commercially available air-liquid interface human nasal culture MucilAir™, offer a more physiologically relevant and robust systems for studying the effects of exposure through inhalation and for studying microbial infections on the nasal cavity. Air-liquid nasal cultures contain a fully differentiated, columnar pseudostratified epithelium consisting of basal cells, ciliated cells, and mucus producing goblet cells; the proportion of which resemble that of the *in vivo* nasal tissue (Constant et al., 2014; Talikka et al., 2014). These culture respond to pro-inflammatory stimuli and the secretion of various chemokines, cytokines, and growth factors have been reported following an exposure to cigarette smoke (CS) (Talikka et al., 2014) or rhinovirus infection (Yu et al., 2011).

Exposure to CS is associated with nasal inflammation (Lee and Kim, 2013; Lan et al., 2007; Huvenne et al., 2010). A possible role of CS exposure in sinonasal cancer has also been discussed (t Mannetje et al., 1999; Kuper et al., 2002; Sham et al., 2010; Moon et al., 2010; d'Errico et al., 2013). Alteration of gene expressions in nasal epithelial cells attributed to smoking resemble that in the lower airway epithelial cells (Sridhar et al., 2008), although some differences exist (Huvenne et al., 2010). Efforts in identifying biomarkers associated with tobacco exposure from the genomic and epigenomic changes in nasal epithelial cells have recently become the focus (Project IV) of the Center for Tobacco Regulatory Science and Lung Health (TCORS)[2]. Therefore, the nasal epithelium is a relevant tissue to evaluate many aspects of the pathophysiological impact of CS on the respiratory system.

Motivated by recent regulatory demands to minimize the use of animals and by an increase in the development of novel tobacco products, a reliable toxicity assessment strategy that is able to determine the pathophysiological risk in human is needed. Although similarities in the nasal passages exist across most mammalian species, striking interspecies differences in nasal architecture are known (Harkema et al., 2006). The nasal (and oral) cavities of humans care capable for both nasal and oral breathing; whereas, most laboratory rodents are nose breathers (Harkema et al., 2006). Therefore to circumvent the interspecies translatability, the aim of the current study was to explore the relevancy of a human 3-D nasal culture model to detect toxicologically relevant findings to assess the biological impact of aerosols generated from a candidate modified risk tobacco product (cMRTP), the Tobacco Heating System (THS) 2.2, as compared with smoke generated from reference cigarette 3R4F. A series of experimental repetitions, where multiple concentrations of THS2.2 aerosol and 3R4F smoke were applied, was conducted to obtain reproducible measurements. The repetitions would allow a more reliable observation and further understanding of the cellular and molecular changes following CS exposure. Aligned with the Vision and Strategy of the Toxicity Testing in the 21st Century (Krewski et al., 2010)—in which animal use should be minimized and mechanistic data should be acquired using human cell-based *in vitro* systems (Sheldon and Cohen Hubal, 2009; Berg et al., 2011; Rovida et al., 2015)—the present study implement a systems toxicological approach where computational biology analyses (i.e., a global analysis of mRNA and miRNA changes using a network-based approach) were used to complement various functional cell-based assays (i.e., cytotoxicity assay, cytochrome P450 activity assay, measurement of secreted pro-inflammatory factors, histological analysis, and cilia beating analysis).

2 Materials and Methods

3R4F cigarettes and THS2.2 tobacco sticks

Two items were assessed in this study: 3R4F cigarettes (University of Kentucky, Kentucky Tobacco Research and Development Center, www.ca.uky.edu/refcig) and the tobacco heating systems (THS)2.2 using tobacco sticks specifically designed to this effect (Philip Morris International R&D). THS2.2 is a heat-not-burn based technology that heats tobacco instead of burning it. Comparative analytical specifications between THS2.2 aerosol and 3R4F smoke was reported before in (Phillips et al., 2016). The 3R4F cigarettes and THS2.2 sticks were conditioned for at least 48 h up to 21 days at 22 ± 1°C with a relative humidity of 60 ± 3% according to ISO standard 3402 (International Organization for Standardization, 1999).

3R4F smoke and THS2.2 aerosol exposure and endpoint generation

A series of five experimental repetitions were conducted. For each of the repetitions, three independent exposure runs were performed (each exposure run was conducted with 28 min continuous exposure to the smoke/aerosol). The duration of exposure was chosen based on the previously reported dose-dependent response of matrix metalloproteinase (MMP)1 secretion; the secretion of MMP1 was considered as a control for the responsiveness of organotypic airway cultures to CS (Mathis et al., 2013).

[2] https://www.med.unc.edu/tcors-lung/research-projects/translational-studies-to-identify-epithelial-biomarkers-of-smoke-exposure

Mathis et al. reported that the highest concentration of secreted MMP1 was observed in a 3-D bronchial culture model following 28 min exposure to 3R4F smoke, as compared with 7, 14, and 21 min of 3R4F exposure.

In the current study, for the exposure runs, each 3R4F cigarette was smoked for 10-11 puffs to a standard butt length (approximately 35 mm) and each THS2.2 was aerosolized up to 12 puffs per THS2.2 stick. The smoking protocol was performed according to the Health Canada smoking regimen (a 55 mL puff over 2 sec, twice per min with an 8 sec pump exhaust time) (Health Canada, 1999).

Within the Dilution/Distribution Module of the Vitrocell® 24/48 exposure system, 3R4F smoke or THS2.2 aerosols were diluted with air to achieve the targeted concentrations. The concentration of nicotine (mg/L) in the 3R4F smoke and THS2.2 aerosol was matched; nicotine was used as the internal reference compound to compare the impact of 3R4F smoke and THS2.2 aerosol (the nicotine yield from one 3R4F cigarette is approximately 1.4 fold greater than from one THS2.2 stick, (Gonzalez-Suarez et al., 2016)). The concentrations were selected based on a dose range finding experiment (data not shown) conducted to identify the maximum tolerable concentration of 3R4F smoke and THS2.2 aerosol. The maximum tolerable concentrations were determined based on the nasal culture morphology where there was no evident morphological damage. Biological test systems (cell cultures) were placed in the Base Module of the Vitrocell® 24/48 exposure system within a climatic chamber), as illustrated in Figure 1.

A pair design was implemented where the exposed samples (to either whole combustible 3R4F smoke or whole THS2.2 aerosol) were exposed with their corresponding air controls during a given exposure run (Fig. 1). Endpoints were measured at various post-exposure time points to assess the responses of the cultures following exposure to 3R4F smoke and THS2.2 aerosol.

3R4F smoke was generated using a 30-port carousel smoking machine (SM) 2000 (Philip Morris International, referred to as "SM 2000-3R4F") connected to a Vitrocell® 24/48 exposure system (Vitrocell® Systems GmbH, Waldkirch, Germany) (Fig. 1). Within one exposure run of 3R4F smoke exposure, tissue cultures were exposed to:

a. A 3R4F smoke dilution to reach a nicotine concentration of 0.15 mg/L smoke, referred to as group "3R4F (0.15),"
b. A 3R4F smoke dilution to reach a nicotine concentration of 0.25 mg/L smoke, referred to as group "3R4F (0.25)," and
c. Undiluted air exposure, referred to as group "3R4F (Air)," which is the air-exposed control.

Another 30-port carousel smoking machine (referred to as "SM 2000-THS2.2") was used to generate THS2.2 aerosol, and connected to another Vitrocell® 24/48 exposure system. Within one exposure run of THS2.2 aerosol exposure, tissue cultures were exposed to:

a. A THS2.2 aerosol dilution to reach a nicotine concentration of 0.15 mg/L aerosol, referred to as group "THS2.2 (0.15),"
b. A THS2.2 aerosol dilution to reach a nicotine concentration of 0.27 mg/L aerosol, referred to as group "THS2.2 (0.27),"
c. A THS2.2 aerosol dilution to reach a nicotine concentration of 0.44 mg/L aerosol, referred to as group "THS2.2 (0.44),"
d. Undiluted air exposure, referred to as group "THS2.2 (Air)," which is the air-exposed control.

An exposure run for 3R4F smoke was performed simultaneously with THS2.2 aerosol (using the dedicated Vitrocell® 24/48 exposure system connected to the specific smoking machine).

Nicotine concentrations of 3R4F smoke and THS2.2 aerosol within the Vitrocell® 24/48 exposure system

Four different trapping experiments were performed throughout the study period (N = 3 trapped columns were collected for each trapping experiment). Because whole smoke/aerosols are trapped in the EXtrelut® 3NT columns (Merck Millipore, Billerica, MA, USA), these trapping experiments cannot be done simultaneously while exposing nasal cultures.

For the trapping experiment, the diluted 3R4F smoke or THS2.2 aerosol was trapped in the exhaust of the dilution/distribution module of the Vitrocell® 24/48 exposure system. The smoke/aerosol was trapped in EXtrelut® 3NT columns soaked with 2 mL of 0.5 M H_2SO_4 solution, as previously reported (Majeed et al., 2014). Nicotine concentrations were measured using gas chromatography–flame ionization detection method. The separation was performed using the Agilent 7890A gas chromatograph (Agilent Technologies, Santa Clara, CA, USA). Peak detection, integration, and quantification of nicotine (according to an internal standard calibration curve) were performed automatically using the Agilent ChemStation software (Agilent Technologies).

Deposited carbonyls in the Vitrocell® base module following 3R4F smoke and THS2.2 aerosol exposure

Ten sampling experiments were conducted throughout the study period. The deposition of various carbonyls were measured in phosphate buffered saline (PBS)-filled Cultivation Base Module following a 28-minute exposure to whole smoke or test aerosol according to the Health Canada smoking regimen (a 55 mL puff over 2 sec, twice per min with an 8 sec pump exhaust time) (Health Canada, 1999). Briefly, before exposure, each row in the Cultivation Base Module of the Vitrocell® 24/48 exposure system was filled with 18.5 mL PBS. Following exposure to diluted 3R4F smoke or THS2.2 aerosol, an aliquot of 1.2 mL PBS-exposed sample (per row) was collected and subjected to a high-performance liquid chromatography (HPLC) coupled with a tandem MS (HPLC-MS/MS) analysis, as previously reported (Majeed et al., 2014).

Organotypic tissue culture models

The organotypic 3-D human nasal epithelial tissue cultures MucilAir™ (Epithelix Sàrl, Geneva, Switzerland) were grown in Transwell® inserts (cat #3470, Corning Incorporated, Tewksbury, MA, USA) and kept in 24-well plates at the air-liquid interface. The nasal MucilAir™ culture models were reconstituted using primary nasal epithelial cells isolated from a healthy 30-year-old male non-smoker donor who underwent surgical lobectomy (the same donor was used for all experiments reported here). The sample was collected according to the Helsinki Declaration on biomedical research and approved by the local ethics commission, as specified by the supplier.

For each of the five experimental repetition, a batch of nasal MucilAir™ was obtained from the supplier. Upon arrival, the nasal MucilAir™ cultures were approximately 45 days old and fully differentiated. They were maintained at 37°C in 0.7 mL MucilAir™ culture medium (the medium was renewed every 48 h according to the supplier's instructions). After four days, the cultures were exposed to 3R4F smoke or THS2.2 aerosol according to the experimental design. Subsequent to the exposure, the cultures were maintained in a new 0.7 mL MucilAir™ culture medium in 24-well plates for up to 72 h post-exposure, after which there was no medium change until samples were collected for various endpoint measurements. Throughout the study, the cultures were monitored routinely by microscopy to detect any bacterial or fungal contamination and to assess their gross morphology.

Adenylate kinase (AK)-based cytotoxicity assay

AK activity in the basolateral medium of the cultures was measured (as a cross sectional sampling at various time points of post-exposure) using a BioVision Bioluminescence Cytotoxicity Assay Kit (BioVision, Inc. Milpitas, CA, USA) or ToxiLight™ bioassay kit (Lonza, Rockland, MA, USA) according to the manufacturers' instruction. The luminescence signal was measured using a FluoStar Omega reader (BMG Labtech GmbH, Ortenberg, Germany). For each of the five experimental repetitions, the value of the luminescence signal was normalized using the mean value of the positive control (Triton X-100-treated cultures; considered as 100% cytotoxicity) and negative control (PBS-treated or untreated cultures; considered as 0% cytotoxicity); the formula is given in the Supplementary Materials and Methods (http://dx.doi.org/10.14573/altex.1605041s). Triton X-100 (1% final concentration) was added to the basolateral media of the cultures for 24 h to maximally induce cell lysis. The mean values of the normalized relative luminescence unit were reported in the figures.

Histology processing

Because major morphological changes were not expected to occur immediately, histological assessment was not performed for the cultures collected at the 4 and 24 h post-exposure time points. Briefly, for the histology processing, 3-D nasal cultures were washed three times with PBS and fixed for 2 h in freshly prepared 4% paraformaldehyde. The fixed cultures were separated from the inserts by detaching the membrane from the plastic with a forceps and bisected at their mid-point prior to processing using Leica ASP300S tissue processor (Leica Biosystem Nussloch GmbH, Nussloch, Germany). The two bisected pieces (per culture sample/1 insert) were embedded into one paraffin block. Microscopy sections of 5-µm thickness were obtained using a microtome and mounted on glass slides. The slides were subsequently transferred to an automated slide stainer Leica ST5020 for staining with hematoxylin (Merck Millipore) and eosin (Sigma-Aldrich, St. Louis, MO, USA) (H&E), and Alcian blue (Sigma-Aldrich). Subsequently, the stained slides were covered with glass coverslip using Leica CV5030 fully automated coverslipper (Leica Biosystem Nussloch GmbH). Digital images were generated using the Hamamatsu NanoZoomer 2.0 slide scanner (Hamamatsu Photonics, K.K., Japan).

Immunostaining and quantification

Immunostaining was automatically performed using the Leica Bond-max autostainer (Leica Biosystem Nussloch GmbH) with the following primary antibodies: anti-Ki67 (Bond™ Ready-to-use Primary Antibody ki67 (K2) (Catalog no. PAO230, Leica Biosystem Nussloch GmbH); anti-p63 (1:100 µL, Abcam-ab735, Abcam, Cambridge, UK); and anti-FoxJ1 (1:2000 µL, Abcam-ab40869, Abcam), as well as the Bond polymer Refine Detection Kit (DS9800, Leica Biosystem Nussloch GmbH). Quantification of p63, ki67, and FoxJ1 immunohistochemistry was performed automatically using Tissue Studio and Image Miner software from Definiens (Definiens AG, Munich, Germany). The number of total nuclei (positively stained and negatively stained nuclei) were automatically calculated by the Definiens software. For a given sample, the proportion of the positive stained cells of each marker was calculated in comparison to the total cell numbers (nucleus).

Cilia beating frequency (CBF)

CBF was measured by placing the cultures in a top-stage incubation chamber (Life Cell Instruments, Seoul, Korea) at 37°C. Cultures were equilibrated for 5 minutes before measurement. CBF was recorded using a digital high-speed video camera (Sony XCD V60, Sony, Tokyo, Japan) connected to an inverted microscope system (Leica DMi8, Leica, Wetzlar, Germany) at a rate of 90 frames per second through an objective lens (4×). A total of 512 video frames were recorded from at least two visual fields (the center of the insert and peripheral). CBF was assessed before exposure, immediately after (0 h post-exposure), 24, and 48 h post-exposure (as a longitudinal measurement from each culture insert). Measuring CBF at 72 h post-exposure present a technical challenge because of the expected time delay associated with the increased number of samples measured at this particular time point. Thus, it was assumed that the CBF alteration at 72 h post-exposure could be inferred from that at 48 h post-exposure.

Automated software CiliaFA was used, which runs on open-source software (ImageJ) (Smith et al., 2012). The software extracts the pixel intensities of the region of interest (ROI) over time from previously recorded video. The CiliaFA Analyser Results Report generated a total of 1600 ROI and converted the pixel intensity into ciliary beating frequency (between 3-52 Hz) based on a signal processing Fast Fourier Transformation (FFT). Subsequently, all 1600 FFT power magnitudes detected, summated to obtain a single power spectrum. For one sample, one spectrum was obtained by determining the mean of all spectra obtained from different visual fields. The spectrum was smoothened by using a moving mean values on 10 points (the delta between points was approximately 0.18 Hz). Finally, the cilia frequency of a given sample was derived from the highest magnitude of the FFT (2.5 Hz was considered the lowest limit of the detected frequency). In a given spectrum, a frequency less than 1.25-times the lowest magnitude was considered noise and not included in the calculation. The FFT power magnitudes was normalized to the ambient noise (the formula is given in the Supplementary Materials and Methods, http://dx.doi.org/10.14573/altex.1605041s). The FFT power magnitudes was subsequently integrated (sum) to those

corresponding to the measured frequency described before. Finally, the summed FFT power magnitudes was normalized to the ambient noise, and to their corresponding air control (within a given exposure run, the pair sample).

Cytochrome P450 (CYP) activity

The activity of CYP1A1/1B1 (combined) was measured using a non-lytic P450-Glo™ assay (Promega, Madison, WI, USA), according to the manufacturer's instruction (as a cross sectional sampling at various time points of post-exposure). Briefly, the luminogenic CYP-Glo substrate luciferin-6' chloroethyl ether (Luciferin-CEE), a substrate for both CYP1A1 and CYP1B1, was added to the basolateral medium, 24 h prior to sample collection. For this reason, the CYP1A1/1B1 activity was not assessed at the 4 h post-exposure time point. The luminescence signal was measured in a FluoStar Omega reader (BMG Labtech GmbH, Ortenberg, Germany). For each of the five experimental repetitions, a positive control of CYP1A1/1B1 activity induction was measured from triplicate cultures treated with 30 nM 2,3,7,8-tetrachlorodibenzo-p-dioxin (TCDD) (Sigma-Aldrich) added to the basolateral media and incubated for 48 h. For the negative control of CYP1A/1B1 activity, luciferin-CEE (substrate only)-treated cultures were used. For each of the five experimental repetition, the CYP1A1/1B1 activity levels were reported relative to the luminescence signals of the mean value of the triplicate positive controls (TCDD-treated tissue inserts were considered as 100% activity induction) and negative controls (considered as 0% activity); the formula is given in the Supplementary Materials and Methods (http://dx.doi.org/10.14573/altex.1605041s). The mean values of the normalized CYP activities are reported.

Luminex-based measurement of secreted analytes

Concentrations of secreted pro-inflammatory mediators were measured in the basolateral medium from the cultures, collected at different post-exposure times (as a cross sectional sampling at various time points of post-exposure). The concentrations of various mediators in basolateral media increased with increasing post-exposure time, and a minimum of 24 h was required for a high probability to exceed the detection limits of the Luminex-based measurement (based on previous observations, data not shown). Therefore, the measurement was not performed in samples collected 4 h post-exposure. The analyte profiling was performed using Luminex® xMAP® technology (Luminex, Austin, TX, USA) and commercially available assay panels (EMD Millipore Corp., Schwalbach, Germany) according to the manufacturer's instructions, to detect: epidermal growth factor (EGF), growth related oncogene alpha, interleukin(IL)6, IL8, macrophage inflammatory protein 3A, MMP1, MMP9, soluble intercellular adhesion molecule (sICAM)1, tissue inhibitor of metalloproteinase (TIMP)1, tumor necrosis factor alpha (TNFA), and vascular endothelial growth factor alpha (VEGFA). The analysis was run on a Luminex®, 200™ or FLEXMAP 3D® reader, equipped with xPONENT software (Luminex, Austin, TX, USA). The capability of the cultures to respond to inflammatory inducers was tested in representative cultures per experimental repetition, in which a set of triplicate samples were treated for 24 h with a combination of TNFA and IL1β (10 ng/ml final concentration for each in the basolateral media). To evaluate the basal levels of secreted mediators, a set of triplicate samples were treated for 24 h with PBS added to the basolateral media (for each of the five experimental repetition). If the measured concentrations were below the limit of detection, a constant value was used (i.e. half of the lower limit of detection).

Statistical analysis

Statistical analysis was performed using SAS software version 9.2 (SAS Institute) on the following data: nicotine and carbonyl measurements, luminescence signals of the AK assay and CYP activity, immunostaining quantification, ciliary beating frequency and power, and the Luminex-based measurement of secreted mediators. Mean values and standard error means are reported (unless otherwise specified). The sample number per endpoints is reported in Supplementary Table 1 (http://dx.doi.org/10.14573/altex.1605041s). Comparisons of an exposed sample versus its air control (i.e., the paired-sample from the same exposure run) were performed using a paired T-TEST. The comparison of 3R4F-exposed versus THS2.2-exposed samples was done after subtracting the values of the corresponding air controls (i.e., the paired sample). Then the comparison was done using a T-TEST corrected for non-equal variance (Satterthwaite correction). Numerical values from secreted mediator analysis (Luminex assay) were transformed using the natural log transformation.

RNA/miRNA purification

Total RNA including microRNA (miRNA) was isolated after washing the culture two times with cold (4°C) PBS at both the basal and apical sides. The cells were then lysed using 700 µL QIAzol™ lysis buffer (Qiagen, Hilden, Germany) followed by RNA extraction using a Qiagen miRNeasy Mini Kit and a QIAcube robot (Qiagen). The quantity of the purified RNA was determined using a NanoDrop™ ND8000 spectrophotometer (Thermo Fisher Scientific, Waltham, MA, USA). The quality of the RNA was analyzed using an Agilent 2100 Bioanalyzer (Agilent Technologies).

mRNA microarray

One hundred ng of total RNA was reverse-transcribed to cDNA using the Affymetrix® HT 3' IVT PLUS kit (Affymetrix, Santa Clara, CA, USA). cDNA was then labelled, amplified to cRNA (complementary RNA), and fragmented. The cRNA concentration in the final hybridization cocktail (50.1 ng/µL) was hybridized into a GeneChip® Human Genome U133 Plus 2.0 Array (Affymetrix). Arrays were washed and stained on a GeneChip® Fluidics Station FS450 DX (Affymetrix) using the protocol FS450_0001 and scanned using a GeneChip® Scanner 3000 7G (Affymetrix). The AGCC software automatically gridded the DAT file image and extracted probe cell intensities into a CEL file. The mRNA array dataset is available in the Arrays Express repository (ID: E-MTAB-4740).

Processing raw CEL files of the mRNA microarray

The raw CEL files were background-corrected, normalized, and summarized using frozen-Robust Microarray Analysis (McCall et al., 2010). Background correction and quantile normalization were used to generate microarray expression values from all arrays passing quality control checks, and was performed using the custom CDF environment HGU133Plus2_Hs_ENTREZG v16.0 (Dai et al., 2005). A log-intensities plot, normalized-unscaled standard error plot (NUSE) , relative log expression plot (RLE), median absolute value RLE (MARLE) and pseudo images using R packages were generated for quality checks (AffyPLM; Bioconductor, Seattle, WA, USA) (Bolstad et al., 2005; Gautier et al., 2004).

CEL files that fulfilled at least one of the quality metric rules described below were dropped for further analyses: a) Pseudo-image displaying a spatial pattern covering approximately 10% of the pseudo-image; b) Median NUSE >1.05; c) |Median RLE| >0.1; and d) (MARLE-median(MARLE))|/ (1.4826 *mad(MARLE)) >1/√0.01, where mad is the median absolute deviation). Subsequently, the RLE and NUSE-based metrics were recomputed, until no more of the CEL file was removed.

For each experimental factor combination item, concentration and post-exposure, a model to estimate the treatment effect was fitted with LIMMA (Smyth, 2004), by including the covariate exposure run as a blocking variable to account for the pairing during an exposure run (exposed vs. air control). The *p*-values for each computed effect were adjusted across genes using the Benjamini-Hochberg false discovery rate method (FDR). Differentially expressed genes were defined as a set of genes whose FDR was < 0.05.

Network Perturbation Amplitude for the analysis of transcriptomics data

The Network Perturbation Amplitude (NPA) methodology (Hoeng et al., 2014; Martin et al., 2012, 2014) aims to contextualize high dimensional transcriptomics data by combining gene expression (log_2) fold-changes into fewer differential node values (one value for each node of a causal biological network model). The collection of causal biological networks used in the study(s) was the human network suite CBN v1.3 (Boué et al., 2015). These networks range between a few dozen and two hundred nodes. Relevant network models considered in this study are listed in Supplementary Table 2 (http://dx.doi.org/10.14573/altex.1605041s). The differential nodes values are determined by a fitting procedure that infers the values that best satisfy the directionality of the causal relationships (positive or negative signs) contained in the network model, while being constrained by the experimental data (the gene log_2-fold-changes, which are described as downstream effects of the network itself). For the NPA scores, a confidence interval accounting for experimental variation and associated *p*-values is computed. In addition, companion statistics, derived to inform on the specificity of the NPA score with respect to the biology described in the network model, are shown as *O and K* if their *p*-values are below the significance level (0.05). A network is considered to be significantly impacted if three values (the confidence interval, *O, and K* statistics) are below 0.05. The detailed methodology was described previously (Hoeng et al., 2014; Martin et al., 2012, 2014).

Gene-Set Analysis of transcriptomics data

Gene-set analysis (GSA) of transcriptomics data was performed using the *Piano* package in the R statistical environment (Varemo et al., 2013). Pathway maps were obtained from the KEGG database (Kanehisa et al., 2014) and exported as R objects into the package *graphite* (Sales et al., 2012). For the GSA, fold-changes were used as gene-level statistics, and the mean was used as the gene-set enrichment score. Statistical significance of the self-contained null hypothesis (Q2) and the gene sampling (Q1) was used to test the null hypothesis (Ackermann and Strimmer, 2009). For each test, the *p*-value was adjusted using the Benjamini-Hochberg procedure.

miRNA microarray

The FlashTag™ Biotin HSR kit (Affymetrix) was used to label miRNA. Two hundred ng of total RNA containing low molecular weight RNA were subjected to a tailing reaction followed by ligation of the biotinylated signal molecule to the target RNA sample. The arrays (miRNA version 4.0) were incubated in a GeneChip® Hybridization Oven 645 (Affymetrix). Arrays were washed and stained on a GeneChip® Fluidics Station FS450 DX (Affymetrix) with protocol FS450_0002 and scanned using a GeneChip® Scanner 3000 7G (Affymetrix). The AGCC software automatically gridded the DAT file image and extracted probe cell intensities into a CEL file.

Processing of raw CEL files of the miRNA microarray

The CEL files were read using the *oligo* package in the Bioconductor suite of microarray analysis tools for the *R* statistical software environment (Carvalho and Irizarry, 2010; Huber et al., 2015; R Core Team, 2013). Quality control (QC) of the miRNA raw data was performed using the *arrayQualityMetrics* package (Kauffmann et al., 2009) based on the following four metrics: (1) the distances between arrays for raw data; (2) the distances between arrays for normalized data; (3) the Normalized Unscaled Standard Errors (NUSE); and (4) the array intensity distributions. Arrays that were outliers in at least two of the metrics were discarded. Subsequently the QC was iteratively rerun on the remaining arrays until all were accepted (362 out of 371). Normalized probe-level data were obtained by applying robust multi-array normalization and summarized at the probeset-level using the median polish method (Bolstad et al., 2003).

Using the annotation provided by Affymetrix and the latest miRNA nomenclature according to miRBase v21 (Kozomara and Griffiths-Jones, 2013), only the probesets pertaining to human were kept in the expression matrix. Only the miRNA probesets with significantly higher intensity values than their matched background probes must be considered as "detected" (Affymetrix miRNA QCT Tool, 2011). A *p*-value threshold of 0.01 was chosen to determine the detection calls based

on Wilcoxon tests. If a miRNA probeset was detected in more than half of the samples in at least one sample group, then it was kept for the further analysis; otherwise, it was discarded; resulting in 527 probesets in the global expression matrix.

For each pairwise comparison, a submatrix was extracted from the global expression matrix by keeping only those samples belonging to the corresponding treatment or control groups, as well as the miRNA probesets that were detected in more than half of the samples in at least one of the two sample groups. A linear models for differential expressions was applied to the resulting submatrices using the moderated t statistics implemented in the limma package (Ritchie et al., 2015). The models included an additional variable to take account the exposure runs. Subsequently, adjusted *p*-values were obtained following multiple testing corrections using the Benjamini-Hochberg FDR (Benjamini and Hochberg, 1995). miRNAs below the FDR threshold of 0.05 were considered to be differentially expressed.

miRNA analysis

To obtain biological interpretation from altered miRNAs, target mRNAs were obtained from the experimentally-derived mRNA target (i.e. the miRNA-mRNA interactions were derived from cross-linking immune-precipitation experiments) (Vlachos et al., 2015). First, to allow a more reliable biological interpretation (avoiding false positive findings), a fold-change threshold was included (Mestdagh et al., 2009): only the differentially expressed miRNAs with $\log_2$fold-changes exceeding 0.33 (those with at least 1.25 fold-changes, in addition to the statistical significance) were included in the analysis. Second, these miRNAs were clustered by Euclidean distance over the 16 fold-change values, resulting in four distinct clusters reported in the present manuscript. Third, the mRNA targets were identified using Diana-TarBase version 7.0 (Vlachos et al., 2015). Fourth, the mRNA targets were further filtered to include only those that were present in our transcriptomic dataset and negatively correlated with the mean of the miRNA fold-changes (coefficient correlation of −0.5), for a given cluster. This approach resulted in a less than 50 potential target mRNA per miRNA cluster (a list of genes is given in Supplementary Tab. 3, http://dx.doi.org/10.14573/altex.1605041s). Enrichment analysis for KEGG pathways was conducted for this list of genes using the EnrichR tool (Chen et al., 2013), in which a standard Fisher exact test combined with a resampling statistics involving random gene sets was used. Pathways with an EnrichR "combined score" > 1.00 were considered and disease specific pathways were excluded (Supplementary Tab. 4, http://dx.doi.org/10.14573/altex.1605041s). Finally, the KEGG pathway classes were reported for each of the miRNA clusters to infer the biological functions of the miRNAs.

Correlation analysis

The robustness of the study design was explored using correlation analyses on the following group of endpoints: 1) functional cell-based assays—which include AK assay, immunostaining quantification, CYP activity, and Luminex-based measurement of secreted analytes—; 2) mRNA profiles; and 3) miRNA profiles. The Pearson and Spearman correlations were computed for each of these endpoint groups by correlating the means of the endpoint values obtained from the experimental repetitions 1 and 2, and the means of those obtained from experimental repetitions 3, 4, and 5.

Before correlating the endpoint values obtained from the functional cell-based assays, the difference (Δ) between the exposed samples and air controls was calculated for each of the concentrations tested, endpoints, and post-exposure time points. To compute the difference (Δ) for AK assay and CYP activity assay, their normalized levels were used (the normalization procedures are described in the Materials and Methods: Adenylate kinase (AK)-based cytotoxicity assay, and Cytochrome P450 activity, respectively). For the immunostaining quantification, the proportion of the positive stained cells was used. For the secreted pro-inflammatory mediators, the logarithmic base 10 of the concentration was used to compute the difference (Δ). Subsequently, for each of these endpoints (for a given concentration and post-exposure time point), the mean value of the differences obtained from the experimental repetitions 1 and 2 were correlated to the mean value from the differences obtained from the experimental repetitions 3, 4, and 5.

To obtain the correlations of the mRNA and miRNA profiles, the fold-changes of mRNA between the exposed samples and air controls were calculated (for a given concentration and post-exposure time point). The mean fold-changes for each mRNA (and miRNA) obtained from the experimental repetitions 1 and 2 were then correlated to the mean fold-changes for each mRNA (and miRNA) obtained from the experimental 3, 4, and 5.

3 Results

3.1 3R4F smoke and THS2.2 aerosol exposure characterization

To assess the biological impact of 3R4F smoke and THS2.2 aerosols, a series of five experimental repetitions was conducted and a collection of results was obtained. These experimental repetitions were performed to increase the robustness of the assessment. Human nasal epithelial cultures (the 3-D MucilAir™ model) were exposed to comparable concentrations of 3R4F smoke and THS2.2 aerosol. A low concentration of 3R4F smoke was applied and matched with a low concentration of THS2.2 aerosol (at a target nicotine concentration of 0.15 mg/L smoke or aerosol). A high concentration of 3R4F smoke was matched with a medium concentration of THS2.2 (at a target nicotine concentration of 0.25 mg/L smoke or aerosol). In addition, a higher concentration of THS2.2 was applied at a target nicotine concentration of 0.44 mg/L aerosol (as described in Materials & Methods). Using the Dilution/Distribution Module of the Vitrocell® 24/48 exposure system, these specific nicotine concentrations were achieved by diluting 3R4F smoke or THS2.2 aerosol during using their exposure to the nasal cultures (Fig. 1).

Throughout the study period, the actual concentrations of nicotine in the applied dilutions of 3R4F smoke and THS2.2 aerosols were monitored through four independent trapping experiments (described in the Materials & Methods: Nicotine

concentrations of 3R4F smoke and THS2.2 aerosol). Table 1 shows that the actual nicotine concentrations closely matched the target concentrations in 3R4F smoke and THS2.2 aerosols. The results show that diluting 3R4F smoke with air at 7-8% in the Dilution/Distribution Module of the Vitrocell® 24/48 exposure system resulted in nicotine concentrations of 0.137-0.156 mg/L. These concentrations of nicotine were comparable to the diluted THS2.2 aerosol at 12.8-13 % (i.e. concentrations of 0.145-0.154 mg/L). Moreover, the higher percentages of 3R4F dilution (13-15%) in the Dilution/Distribution Module resulted in nicotine concentrations of 0.240-0.263 mg/L. These concentrations were similar to the THS2.2 aerosols at 22.6-24.0% (i.e. concentrations of 0.260-0.292 mg/L).

To characterize the deposition of various carbonyls following the exposure using Vitrocell® 24/48 exposure system, PBS-filled Cultivation Base Module were used. The PBS-filled Cultivation Base Module were then exposed to the applied dilutions of 3R4F smoke and THS2.2 aerosol for 28 min. These sampling were assessed throughout the study period (N = 10 samplings were conducted). At the comparable levels of nicotine concentrations (i.e. between (3R4F (0.15) and THS2.2 (0.15); and between 3R4F (0.25) and THS2.2 (0.27)), the deposited concentrations of various carbonyls were lower in the PBS exposed to THS2.2 aerosol, as compared with that exposed to 3R4F smoke (Fig. 2). A concentration-dependent increase of deposited carbonyls in PBS was observed following exposure to THS2.2 aerosol when it was applied up to a concentration of 0.27 mg nicotine/L aerosol. Whereas, no marked increase in the deposited carbonyls was observed when the THS2.2 aerosol was applied at a nicotine concentration of 0.44 mg/L (i.e., THS2.2 (0.44)) (Fig. 2).

3.2 Cytotoxicity and tissue morphology

At various time-points after exposure, cytotoxicity associated with 3R4F smoke and THS2.2 aerosol exposure was assessed. Cytotoxicity was measured using an adenylate kinase (AK) released-assay. AK is released into the basolateral media of the nasal cultures upon cell membrane damage. At 4 h post-exposure, the cytotoxicity levels across all groups were not significantly different (Fig. 3A). At later time points after exposure (24, 48, and 72 h), greater cytotoxicity levels were observed in the 3R4F (0.25) group compared with air controls. In contrast, no difference was observed across the THS2.2 exposed groups (at all concentrations and all post-exposure time points tested), relative to air control.

Histological assessment was performed to assess the impact of exposure on the morphology of the cultures post-exposure (Fig. 3B,C). At 48 and 72 h post-exposure, a marked thinning of the epithelium was only observed in 3R4F (0.25) group (Fig. 3B,C).

To evaluate further the possible adverse effects of THS2.2 aerosol, a dose range assessment was conducted. A broader range of THS2.2 concentrations were exposed to the nasal cultures. Various dilutions of THS2.2 were applied to the cultures using the Vitrocell® 24/48 exposure system, corresponding to the concentrations of nicotine between 0.15 mg/L and 1.79 mg/L (the experimental procedure of the exposure run and the summary endpoints is reported in Supplementary Fig. 1, http://dx.doi.org/10.14573/altex.1605041s). Culture morphology and cytotoxicity were assessed at 72 h post-exposure. This dose range assessment showed that the cultures exposed to THS2.2 aerosol at concentrations above 1 mg nicotine/L aerosol exhibited morphological changes (Fig. 4). The AK assay-based cytotoxicity also showed 15 -35% increases in cytotoxicity following THS2.2 aerosol exposure at concentrations of 1.02 and 1.79 mg nicotine/L, as compared with air controls.

3.3 Immunostaining analysis

Immunostaining was performed to evaluate whether the proportions of different cell types were impacted by the exposure. The expression of p63, Ki67, and FoxJ1 in the culture sections were examined to detect basal cells, proliferating cells and columnar ciliated cells, respectively. Immunostaining was not performed the tissues exposed to the higher concentration of 3R4F (i.e., 3R4F (0.25) group) because most of the tissue sections showed substantial tissue damage (Fig. 3B, C). Quantification of the staining was expressed as a proportion of the positive-stained cells respective to the total cell numbers per tissue section, and as compared with the air control.

Figure 5A shows that the p63 immunostaining was confined to the basal cells and Ki67 was mostly limited to the basal cells. For the cultures collected at 48 h post-exposure, decreased levels of Ki-67-stained cell proportion were observed upon 3R4F and THS2.2 exposure (Fig. 5B). However, relative to air controls, 3R4F smoke exposure caused a greater reduction of the Ki-67 proportion as compared with the reduction following THS2.2 (at all concentrations tested).

At 72 h post-exposure, a lower proportion of FoxJ1-positive stained cells was observed in the 3R4F (0.15) group, as compared with the air control (Fig. 5C). No substantial changes were observed upon THS2.2 exposure.

3.4 Cilia beating of the nasal cultures

Cilia beating frequency (CBF) levels were first monitored before the cultures were exposed to 3R4F smoke or THS2.2 aerosol. This first measurement was done to assess the variability of baseline cilia beating levels. The impact of exposure on CBF was then evaluated immediately after exposure (referred to as 0 h post-exposure), and at 24 and 48 h post-exposure. Figure 6A (*left panels*) shows that the detected CBF levels before exposure were comparable across all groups (approximately between 6-8 Hz).

Immediately after exposure (0 h post-exposure), 3R4F (0.15)-exposed cultures had reduced levels of CBF as compared with the air control. A further reduction of the CBF was observed in the 3R4F (0.25) group. At 24 and 48 h post-exposure to 3R4F (0.25), the CBF levels were comparable to the air control. THS2.2 aerosol exposure, at all post-exposure time-points, was linked to minimal changes of CBF levels, as compared with the air control.

The power magnitudes of the detected signal (FFT power magnitudes) are reported in Fig. 6A (*right panels*). The power of the detected CBF signal was reduced in a concentration dependent manner following 3R4F smoke exposure. Furthermore, following THS2.2 aerosols exposure, the power of the detected signals was minimally altered (at all concentrations tested and all post-exposure time points) relative to the air controls.

3.5 Alterations of CYP1A1/CYP1B1 activity

Cytochrome P450 (CYP) 1A1 and 1B1 metabolize toxicants found in CS, such as polycyclic aromatic hydrocarbons (PAHs), nitrosamines, and arylamines. CYP1A1 is the most actively studied human pulmonary CYP because of its importance in PAH metabolism (Hukkanen et al., 2002). CYP1A1 is inducible by benzo-(a)pyrene in primary human nasal epithelial cells *in vitro* (Baulig et al., 2003). CYP1B1 is expressed in human lung tissues and is inducible by smoking; it also metabolizes PAHs (Hukkanen et al., 2002). In the present study, the impact of exposure on the activity of CYP1A1/CYP1B1 (combined) was assessed at 24, 48, and 72 h post-exposure (Fig. 6B).

At 24 h post-exposure, both 3R4F and THS2.2 did not substantially impact the activity of CYP1A1/CYP1B1, relative to air controls. At 48 and 72 h post-exposure, 3R4F (0.15)-exposed cultures had a greater level of CYP1A1/CYP1B1 activity than the air controls (Fig. 6B). Upon exposure to the higher concentration of 3R4F (i.e., 3R4F (0.25)), the levels of CYP1A1/CYP1B1 activity were comparable to that of the air control (at 48 and 72 h post-exposure). Furthermore, no substantial alterations in CYP1A1/CYP1B1 activity were observed across all groups following THS2.2 aerosol (at all concentrations tested).

3.6 Profiles of secreted pro-inflammatory mediators following exposure

To determine the impact of 3R4F smoke and THS2.2 aerosol on the secretion of pro-inflammatory mediators, the concentrations of cytokines, chemokines, and growth factors were measured in the basolateral media of nasal cultures at various post-exposure time points (as a cross sectional sampling).

At a given post-exposure time point, with an increasing concentration of 3R4F exposure, increased concentration of pro-inflammatory mediators were measured in the basolateral media (Fig. 7A). However, the secreted levels of TIMP1, VEGFA and IL6 protein were not altered in a concentration-dependent manner in the 3R4F-exposed cultures. The longer the post-exposure time, the greater the concentration of the secreted mediators; this was particularly evident in the 3R4F-exposed cultures. Following THS2.2 exposure (at all concentrations and post-exposure time points), modest changes of the mediator levels were observed as compared with the air controls. Only the secreted levels of VEGFA were increased in a concentration-dependent manner in the THS2.2-exposed cultures.

The exposure-induced impact (i.e. fold-changes as compared with their corresponding air controls) is shown in Fig. 7B. The fold-changes of each of the mediators relative to their respective air controls are displayed as heatmaps. The heatmaps display a pattern of the increasing fold-changes following 3R4F smoke.

3.7 Exposure impact on global mRNA profiles

Molecular alteration in already damaged tissues simply indicate the presence of tissue injury that had occurred (Davis et al., 2013). Therefore, transcriptomic profiles from such tissues cannot infer the toxicity-related mechanisms of exposure. In this study, an investigation of the possible toxicity-related mechanisms following 3R4F smoke of THS2.2 aerosol exposure was performed using cultures that remained intact (or minimally damaged): 3R4F (0.15); THS2.2 (0.15), THS2.2 (0.27); THS2.2 (0.44) groups.

Volcano plots showing changes of gene expression in nasal cultures following 3R4F and THS2.2 exposure are shown in Fig. 8A. For a given exposure condition (an exposed sample vs. the air control, at a given post-exposure time point), the alteration of gene expression (increase or decrease) with the $-\log_{10}$ adjusted (FDR) *p*-value statistics are shown. The plots demonstrate that at the earliest post-exposure time (4 h), a more robust alteration of gene expression was observed for 3R4F and THS2.2 groups. At longer duration post-exposure, fewer alterations in gene expression were observed.

To infer the biological effects of exposures from the transcriptomics data, a network-based systems biology approach was conducted. This approach uses biological network models that contain a series of cause-and-effect relationships (Boué et al., 2015). The network models can be grouped into network families, representing more general biological processes (e.g., Cell Proliferation, Cell Fate, Cell Stress, or Inflammatory Process Networks network families). The nodes of the networks correspond to biological entities (e.g., protein abundances, protein activities, chemical compounds, or biological processes-described as molecular entities) (Hoeng et al., 2014; Boué et al., 2015). Each of the edges in the network models carries a causal directionality between two nodes based on information reported in the scientific literature (Hoeng et al., 2014; Boué et al., 2015). For many nodes, this literature-derived information supporting the relationship between a node and the expression of certain genes is available. Therefore, a collection of transcriptome data (exposed vs. control samples) can be used to predict computationally the activity/functionality of the node. A quantitative approach to infer an impact of exposure using the collection of biological network models was previously developed and reported: the Network Perturbation Amplitude (NPA) approach (Hoeng et al., 2014). The algorithm is based on backward reasoning, where the changes in gene expression are considered as a consequence of the activity of an "upstream" node. Finally, the predicted activation or inhibition of the backbone nodes and the causality of the network edges permit inference and computation on the network as a whole. Using this approach, Figure 8B shows the NPA scores for the various biological network models that were perturbed following exposure as compared relative to the air controls.

The impact of exposure on the nasal cultures (perturbed network scores) decreased with duration of the post-exposure time (Fig. 8B). At a given post-exposure time point, the majority of the networks were perturbed by a greater magnitude following exposure to 3R4F (0.15) compared with THS2.2 (0.15), THS2.2 (0.25), and THS2.2 (0.44).

Within the Cell Fate network family, 3R4F (0.15) exposure was linked to a sustained perturbation—impacted at all post-exposure time points—of Senescence, Response to DNA Damage, and Apoptosis networks (Fig. 8B). Within the Cell Proliferation network family, a sustained impact of 3R4F (0.15) on MAPK, Jak Stat, and Growth Factor networks was observed. Moreover, within the Cell Stress network family continuous perturbations of Xenobiotic Metabolism Response, Oxidative Stress, and NFE2L2 Signaling networks were observed following 3R4F (0.15). Finally, all networks within the inflammatory processes network family—Tissue Damage, Epithelial Mucus Hypersecretion, and Epithelial Innate Immune Activation—were impacted by 3R4F (0.15), at all post-exposure time points.

At a comparable nicotine concentration (0.15 mg nicotine/L), the pattern of the THS2.2-induced network perturbation in the nasal cultures was different from that of 3R4F (0.15): THS2.2 (0.15) was only linked to significant NPA scores at 4 h post-exposure time points. A transient impact was observed; most of the network models were no longer significantly perturbed at 48–72 h post-exposure. When THS2.2 aerosols were applied to the nasal cultures at higher concentrations of nicotine (0.27 and 0.44 mg nicotine/L aerosol), increased NPA scores were observed. These results indicated a concentration-dependent increase of the THS2.2-induced perturbations.

A complementary biological interpretation of the transcriptome data was performed using enrichment analysis. Figure 9 shows a selected collection of the KEGG pathways: the heatmap displays selected KEGG pathways that were analogous to the network models (Fig. 9; the network names are given in square brackets, [ ]). If the analogous network model was not available, a network model that was closely related to the KEGG pathway was assigned. For example, if the key molecules being described in a network model (http://www.causalbionet.com/) resemble the biology described for a particular KEGG pathway (http://www.genome.jp/kegg/pathway.html), the network model was considered analogous. A complete list of the KEGG pathways obtained from the enrichment analysis is shown in Supplementary Fig. 2 (http://dx.doi.org/10.14573/altex.1605041s).

Figure 9 shows that 3R4F (0.15) exposure was associated with a significant enrichment of many of the KEGG pathways at 4, 24, 48, and 72 h post-exposure. At a comparable nicotine concentration, THS2.2 (0.15) aerosol was linked to significant enrichment of KEGG pathways, particularly at 4 h post-exposure. When the nicotine concentration in the THS2.2 aerosol was applied at a concentration of 0.44 mg nicotine/L aerosol (i.e. the THS2.2 (0.44) group), significant enrichment of the "Metabolism of xenobiotics by cytochrome P450" and "HIF-1 signaling pathway" was observed at all post-exposure time points.

3.8 Exposure impact on global miRNA profiles of the nasal cultures

miRNA, a regulator of gene expression, influences many biological processes (Pritchard et al., 2012). To complement the analysis (based on the cultures' transcriptome profiles described above), miRNA profiles of the nasal cultures were obtained. Similar to the transcriptome analysis, by which deriving information from damaged tissue was avoided, the miRNA expression profiles from the following groups was derived: 3R4F (0.15); THS2.2 (0.15); THS2.2 (0.27); and THS2.2 (0.44) groups (as compared with the air control).

The alterations of miRNA upon exposure (relative to the air control) are displayed as volcano plots in Fig. 10A. Different from the mRNA profile pattern following 3R4F (0.15) smoke exposure, the miRNA profile was altered to a greater degree at 72 h post-exposure than at earlier time points (i.e. a greater number of the significantly altered miRNAs was detected). However, following THS2.2 (0.25) and THS2.2 (0.44) aerosols, more miRNAs were significantly altered at 4 h post-exposure than at the later time points.

To determine biological insights from the miRNA alterations, significantly altered (FDR p-value < 0.05 and with fold-changes of at least 0.33) were clustered. They were then uploaded to Diana-TarBase, from which the miRNA target genes were subsequently identified (described in Materials & Methods). These target genes (per miRNA cluster) were then subjected to an enrichment analysis. Figure 10B shows which classes of the KEGG pathways were enriched and associated with each of the miRNA clusters. The downregulated of miRNAs within cluster A and C were linked to cellular metabolism (supported by the annotations "amino acid metabolism", "carbohydrate metabolism", "lipid metabolism", "translation" and "transcription"). These pathways were linked to a cellular response toward environmental stressor (as evidenced by the annotation "environmental adaptation"). Moreover, the upregulation of miRNAs within cluster D was associated with cellular interaction ("cellular community" and "signaling molecules and interaction") and "lipid metabolism." The increased levels of miRNA within cluster B (i.e. miR-4521) were not linked to a particular cellular process.

Robustness of the study design: Correlation of the outcomes across the experimental repetitions

The present study comprised five experimental repetitions in which the impact of 3R4F smoke and THS2.2 aerosols on a nasal 3-D culture model was assessed. The collection of endpoints described before were obtained across these experimental repetitions. For each of the repetitions, a batch of 3-D nasal cultures was obtained from the supplier. To explore the variability and robustness of the observation across the experimental repetitions, a correlation of the endpoint values was conducted.

First, a correlation of the endpoint values from various functional cellular assays (i.e. immunostaining, AK assay, CYP1A1/1B1 activity assay; and Luminex-based measurement of pro-inflammatory mediators) were computed. To achieve this, the difference (Δ) for each of these endpoints and post-exposure time points between the exposed samples and air controls was calculated (described in Materials and Methods: Correlation analysis). Subsequently, a mean value was calculated for the experimental repetitions 1 and 2 (the x-axis in Fig. 11) and for experimental repetitions 3, 4, and 5 (the y-axis in Fig. 11). The plots are separated into stimulus exposure type. They illustrate that these mean values obtained from the experimental repetition 1 and 2, were correlated to those obtained from the experimental repetition 3, 4, and 5. Greater correlations were observed for 3R4F

smoke exposure as compared with THS2.2 aerosol exposure. This was consistent with the increased alterations of these endpoint values upon 3R4F exposure (greater cytotoxicity, greater alteration of CYP1A1/1B1 activity, and greater secretion of pro-inflammatory mediators) than upon THS2.2 exposure.

Second, correlation plots were generated to assess the reproducibility of the gene-expression changes obtained from the different experimental repetitions. The gene expression data from experiments 1 and 2 were combined, and subsequently the mean fold-changes for each gene in this combined dataset was obtained (the x-axis in Fig. 12). Similarly, the gene expression data from experiments 3, 4, and 5 were combined, and subsequently the mean fold-changes for each gene in this combined dataset was obtained (the y-axis in Fig. 12). Finally, correlation plots for the different comparisons were generated with each dot in the correlation plots representing an individual gene (mRNA). Figure 12 displays only representative groups that were greatly perturbed following exposure (as reflected by the volcano plots in Fig 8A). The correlation plots for all groups are reported in Supplementary Fig. 4 (http://dx.doi.org/10.14573/altex.1605041s).

The plots (Fig. 12) show that at 4 h post-exposure, gene expression changes in tissues exposed to 3R4F (0.15) were correlated between those obtained in experiments 1 and 2 and those obtained in experiments 3, 4, and 5 (Pearson correlation of 0.83). Furthermore, the gene expression changes of THS2.2 (0.15), THS2.2 (0.27), and THS2.2 (0.44) were correlated between those obtained in experiments 1 and 2 and those obtained in experiments 3, 4, and 5. The Pearson correlations of the THS2.2-associated fold-changes were lower than for 3R4F (0.15) because of the lower levels of gene alterations as shown by the volcano plots (see Fig. 8A).

A similar approach to that assessing the reproducibility of the mRNA changes was used to assess the reproducibility of the miRNA expression changes obtained from the different experimental repetitions. The miRNA expression data from experiments 1 and 2 were combined and used to compute a single value of fold-changes for each of the detected miRNAs (the x-axis in Fig. 13). Similarly, the combined data from experiments 3, 4, and 5 were used to compute a single value of the fold-changes of the miRNA (the y-axis in Fig. 13). Last, correlations between the fold-changes for all detected miRNA in the datasets were computed for each comparison. Figure 13 displays only representative groups that were greatly perturbed following exposure (as reflected by the volcano plots in Fig. 10A). The correlation plots for all groups are reported in Supplementary Fig. 5 (http://dx.doi.org/10.14573/altex.1605041s).

The plots (Fig. 13) show that at 72 h post-exposure, the miRNA expression changes in tissues exposed to 3R4F (0.15) were correlated between those obtained in experiments 1 and 2 and those obtained in experiments 3, 4, and 5 (Pearson correlation of 0.55). Furthermore, the miRNA expression changes in the THS2.2-exposed groups across the experimental repetition did not show high correlation values because of the low changes in miRNA expression in these groups as evidence the volcano plots in Figure 10A.

4 Discussion

Advances in the field of *in vitro* toxicological testing are motivated by the principle of the Three Rs (Balls, 2010) and the 21st Century Toxicology framework—, in which animal use should be minimized and mechanistic data should be acquired using human cellular-based *in vitro* systems (Sheldon and Cohen Hubal, 2009; Berg et al., 2011; Rovida et al., 2015). Moreover, with the increasing concern about toxicity impact of particle exposure via inhalation, non-animal alternative methods that are appropriate for predicting respiratory toxicity effects in humans are needed. Here, we report our study that are aimed to explore the relevancy of a human 3-D nasal culture model to detect toxicologically relevant findings to assess the biological impact of aerosols generated from a candidate modified risk tobacco product (cMRTP), THS2.2, as compared with smoke generated from reference cigarette 3R4F. Human nasal epithelium is the first barrier against inhaled toxicants, and thus is relevant for the toxicological assessment of CS and tobacco heated aerosol.

To minimize the variabilities and increase the robustness of the assessment, this study comprised five experimental repetitions. The repetitions were performed within an approximate twelve-month period. For each of the repetitions, a new batch of nasal cultures was obtained from the supplier. The nasal epithelial tissue cultures used in this study were reconstituted from primary nasal epithelial cells of a single donor: a 30 year-old male nonsmoker. Although the use of single donor has the potentially drawback of only capturing the donor-specific response, we chose to use one donor to reduce the impact of donor-to-donor variability. Future studies using a larger number of donors could be done to confirm the observations reported here. The results reported here are aggregated data collected throughout the study period (described in Materials & Methods). For each of the exposure run performed using the Vitrocell® 24/48 exposure system, air-exposed cultures were always included (referred to as the air control). The air control was used to confine the effect of the experimental exposure. Moreover, the study was designed such that the batch effect could be reduced; for example, the variability of the culture batch, operator, reagent, and day of the exposure run and sample collection. These variabilities may lead to improper biological conclusions, because observations caused by the batch effect cannot be distinguished from real biological effects. To explore the associations across the experimental repetitions, correlation analyses of the various endpoint values were reported. The correlation analyses indicated that the results obtained from the different experimental repetitions were correlated, although we acknowledge that additional sources of variabilities might exist.

The biological impact of THS2.2 aerosol was assessed relative to that of 3R4F smoke by applying the exposure to the nasal culture at the comparable nicotine concentrations. Nicotine was chosen as the internal reference compound to enable a fair comparison between THS2.2 aerosol and 3R4F smoke. The target nicotine concentrations were monitored throughout the study via multiple trapping experiments, where the diluted 3R4F smoke or THS2.2 aerosol was trapped in the EXtrelut® 3NT column.

We observed that the applied dilutions of 3R4F smoke and THS2.2 aerosols were similar to the intended target nicotine concentrations. Additional characterization of the smoke/aerosol involved the measurements of representative carbonyls deposited in the Base Module of the Vitrocell® 24/48 exposure system. For carbonyl measurement, the Base Module was filled with PBS and these PBS-exposed samples were then collected throughout the study period (ten samplings were conducted throughout the study period). The concentrations of the representative carbonyls that were deposited in the PBS samples following 28 min exposure to the highest concentration of 3R4F (at a nicotine concentration of 0.25 mg/L), were 3.7-10.3 fold greater than those in the PBS samples exposed to the comparable nicotine concentration of THS2.2 (at a nicotine concentration of 0.27 mg/L).

Pronounced biological effects associated with exposure observed by histological analysis and AK assay, both of which revealed the epithelium morphology and cytotoxicity, respectively. Thinning of the nasal epithelium was observed in H&E-stained sections of cultures exposed to 3R4F smoke at a nicotine concentration of 0.25 mg/L (i.e. the 3R4F (0.25) group). The morphological changes following 3R4F smoke 0.25 mg nicotine/L (equivalent to 14% 3R4F smoke dilution) were consistent with our previous findings, where we observed that 15% 3R4F smoke dilution resulted in thinning of the human 3-D bronchial epithelial models (Iskandar et al., 2015). The current study further showed an increase of cytotoxicity by 30-40% in 3R4F (0.25)-exposed cultures relative to the air control. Elevated cytotoxicity levels were not detected at earlier post-exposure time points (4 h) and were only observed at the 24, 48, and 72 h post-exposure time points. The delayed response (increased levels of cytotoxicity at later post-exposure time points) suggests the inability of the nasal cultures to recover fully from 3R4F smoke-induced toxicity. When THS2.2 aerosol was applied at a comparable nicotine concentration (0.27 mg nicotine/L), thinning of the nasal epithelium was not observed. At all post-exposure time points, AK-based cytotoxicity levels of the THS2.2 (0.27)-exposed cultures were similar to the air controls. When THS2.2 aerosols were applied at nicotine concentrations above 1 mg/L, morphological changes and increased cytotoxicity levels were observed. Altogether, these results suggest that at least a 4-fold increase of nicotine concentrations in THS2.2 aerosol were required to elicit similar morphological changes/cytotoxicity in the nasal cultures exposed to 3R4F smoke.

Reduced proportions of Ki67-positive stained cells were detected in sections of nasal cultures exposed to THS2.2 (0.15) and THS2.2 (0.27) aerosols: reductions of 20–22% (at 48 h post-exposure) and 8–28% (at 72 h post-exposure) were observed compared with the air control. The reduced proportions of Ki67-positive stained cells relative to the air control were similarly observed in the 3R4F (0.15)-exposed cultures. However, this 3R4F (0.15)-induced reduction of Ki67 proportions occurred to a greater extent (reduced by 34%). This finding is in contrast to our previous *in vitro* observation following repeated CS exposure, where increased Ki67-positive stained cells were observed in human 3-D nasal and bronchial epithelial culture models (Talikka et al., 2014). Ki67 is a proliferation marker and a known driver of the cell cycle (Szabo, 2001). Increased proliferation in airway epithelial cells is considered to be a reliable indicator of many airborne chemical toxicants (Calderón-Garcidueñas et al., 1999). Our present finding is also in contrast with that observed *in vivo* following airborne insults. In severe asthma or upon allergen challenge, airway epithelial cells proliferated at a much higher rate than in normal individuals (Cohen et al., 2007). The discrepancy between the current study and previous findings may be attributed to i) the mode of exposure (acute vs. repeated), and ii) an increase of mucus-producing cells to shield the epithelium from toxic exposure (Harkema et al., 2006). Previously, Harkema et al. reported that acute/short-term exposure to ozone may reduce the proliferative capacity of nasal epithelia, while the number of mucus-producing cells increased correspondingly to protect the epithelium (Harkema et al., 2006). Similarly, our data showed that a decline in the proportion of Ki67-positive stained cells was transient (only observed at 48 h, but not at 72 h post-exposure), and was complemented by an upregulation of the expression of the MUC5AC gene—a specific marker for secretory-goblet cells (Ding and Zheng, 2007) (Supplementary Fig. 3, http://dx.doi.org/10.14573/altex.1605041s).

The present study showed a marked reduction of the detected CBF immediately (0 h) after exposure to 3R4F (0.25) smoke. This reduced frequency level was likely linked to the overt morphological changes discussed before (thinning of the nasal epithelium cultures). Although the results suggest that the CBF of the 3R4F (0.25)-exposed cultures returned to levels comparable to the air controls over time (at 24 and 48 h post-exposure), the power magnitudes (i.e. detected cilia-beating signals) were significantly reduced. Therefore, this result inferred that the proportion of cilia on the surface of the 3R4F (0.25)-exposed cultures were greatly reduced over the post-exposure time points studied. The reduced CBF is in agreement with other *in vivo* and *in vitro* studies, indicating the negative impact of CS on mucociliary clearance (Stanley et al., 1986; Kreindler et al., 2005; Cohen et al., 2009). Normal mucociliary clearance is dependent upon a proper ciliary beating and the biological properties of the airway surface liquid (Cohen et al., 2009; Virgin et al., 2010), and acts as an initial defense mechanism to clear inhaled toxicants from the nasal passages (Harkema et al., 2006). The reduced CBF (and the power of the detected signals) in the 3R4F (0.25)-exposed cultures was consistent with the observed reduced proportion of FoxJ1-positive stained cells. FoxJ1, a marker for ciliated cells, is a transcription factor that regulates cilia-related genes (Brekman et al., 2014). Overexpression of FoxJ1 was reported to halt the CS extract-mediated inhibition of cilia growth in differentiating normal human airway basal cells (Brekman et al., 2014). Smoking is also associated with a shortening of airway cilia (Leopold et al., 2009; Brekman et al., 2014). In contrast, following THS2.2 aerosol exposure, the frequencies of cilia beating and the power of the detected signals were not significantly different from those of the air control. Moreover, the proportions of FoxJ1-positive stained cells in the THS2.2 exposed tissues (at all concentrations tested) were not significantly altered. Altogether, the impact of 3R4F smoke exposure on the ciliary function of nasal cultures was more pronounced compared with THS2.2 aerosol exposure (at all tested concentrations).

Our results indicated that the prominent 3R4F (0.25)-induced toxicity (thinning of the nasal epithelium cultures and increased cytotoxicity level) also impacted the metabolic capacity of the cultures, i.e. the culture capability to metabolize nitrosamines and polycyclic aromatic hydrocarbons, which are abundant in CS (Hukkanen et al., 2002). At 48 and 72 h post-exposure, the activity of CYP1A1/CYP1B1 in the 3R4F (0.25)-exposed cultures were observed to be comparable to the air controls. This finding is consistent with our previous observations in human 3-D bronchial culture models (Iskandar et al., 2015).

CYP1A1 and CYP1B1 are the major enzymes that metabolize nitrosamines and PAHs abundant in CS (Hukkanen et al., 2002). CS exposure is linked to the increased CYP1A1/CYP1B1 activity (Hukkanen et al., 2002; Hussain et al., 2014). Moreover, in 3R4F (0.15)-exposed cultures, where the epithelium remained intact (no thinning), a 12% increase in CYP1A1/CYP1B1 activity was detected in the 3R4F (0.15) group at 48 and 72 h post-exposure. In contrast, the levels of CYP1A1/CYP1B1 activity in THS2.2-exposed cultures (at all concentrations tested) were nearly comparable to the air control. These results suggested a lower presence of nitrosamines and polycyclic aromatic hydrocarbons in THS2.2 aerosol, as compared with that in 3R4F smoke (at all concentrations tested).

Although the impact of 3R4F (0.15) did not cause overt morphological changes in the cultures—as assessed by the histology analysis and AK assay—,the systems level (omics) analyses demonstrate global mRNA (and miRNA) alterations, relative to the air controls. The network-based systems biology analysis indicated that almost all biological network models were significantly perturbed following 3R4F (0.15) exposure. The degree of biological impact (evidenced by the scores of NPA) was at the highest at 4 h post-exposure and diminished with increasing post-exposure time. These observations suggested that the cultures could eventually cope with the exposure-induced impact over time (or were capable of initiating a repair mechanism). This fading pattern of the biological impact over post-exposure time is in agreement with our previous observation where an exposure of 8% 3R4F smoke (containing a nicotine concentration of approximately 0.15 mg/L) was linked to a declining biological impact on *in vitro* human 3-D bronchial epithelial cultures (Iskandar et al., 2015). Furthermore, the current study shows that THS2.2 aerosol exposure (all concentrations tested) was also associated with a declining impact on the network perturbation/biological pathways. Interestingly, the scores of the network perturbation following THS2.2 aerosol exposure waned more rapidly than those following 3R4F (0.15) over increasing post-exposure time. Therefore, the 3R4F-induced impact on nasal cultures was greater than the THS2.2-induced impact, indicating that the nasal cultures could cope better with THS2.2 aerosol exposure than with 3R4F smoke. Furthermore, to complement and support the network-based analysis, we conducted a gene-set analysis using a previously published method (Varemo et al., 2013). The gene set analysis was performed to identify various biological pathways that were enriched in the dataset (exposed vs. air control). The gene-set analysis provided a similar finding to the previous study, where fewer pathways were enriched by 3R4F (0.15) at the 72 h post-exposure time point. Likewise, the gene-set analysis demonstrated that THS2.2 aerosol exposure was predominantly linked to various KEGG pathways only at the 4 h post-exposure time point. Additionally, the analysis of miRNA suggested a more pronounced effect of 3R4F smoke on altered miRNA expression profiles of the nasal cultures as compared with the THS2.2 aerosols.

The increased level of secreted TIMP1 and VEGFA with increasing duration of post-exposure in the basolateral media of the exposed tissues (i.e. 3R4F (0.15) and THS2.2 aerosol (at all concentration tested) further substantiates the notion of activation of a cellular repair response. Normally, TIMP1 is constitutively expressed at low levels in airway epithelium (Chen et al., 2008). In various wound healing and disease models, the expression of TIMP1 in epithelial cells increases during regeneration (Chen et al., 2008). Moreover, the role of VEGFA in tissue repair is linked to increased compensatory growth during repair processes (Marwick et al., 2006). These elevated levels of secreted TIMP1 and VEGFA were also observed previously in human 3-D bronchial culture models exposed to 8% 3R4F (with a nicotine concentration of approximately 0.15 mg/L) (Iskandar et al., 2015). Differently, upon a higher concentration of 3R4F (at a nicotine concentration 0.25 mg/L), which was associated with pronounced epithelium thinning and cytotoxicity, the secretion TIMP1 and VEGFA did not increase over the post-exposure time. This observation further strengthen the argument regarding the inability of the nasal culture to cope with 3R4F (0.25)-induced toxicity. These results imply that to preserve the capacity of the nasal cultures to cope with exposure-induced injury, 3R4F smoke should be applied at a nicotine concentration at least 4-times lower than that of THS2.2 aerosol.

The relevancy and applicability of an *in vitro* human 3-D nasal epithelial culture model as a test system for a toxicity assessment of inhalation exposure, have been demonstrated in this present study. With the increasing concerns about the effects of ambient particles on the respiratory systems—nanoparticles, cosmetics, atmospheric pollutants, dusts, CS, and new generation of tobacco products—and pressure to find non-animal alternative test systems, available *in vitro* models of the respiratory tract should be assessed particularly for predicting the effects in humans. The use of animal models for studying the respiratory pathophysiology has produced variable results mainly due to interspecies differences in the anatomy and histology of the respiratory system (e.g. ratios of cell types, CYP activities, airway architecture) (BéruBé et al., 2009). The systems toxicological approach applied in this study (the combination of functional cell-based assays and computational approaches) enabled a comprehensive impact assessment of THS2.2 aerosol as compared with 3R4F smoke. Future studies may incorporate an assessment of DNA methylation profiles following THS2.2 aerosol and 3R4F smoke. The integration of multi-modality data will offer a more comprehensive overview of tissue responses following exposure.

Nevertheless, the present study suggested a minimal set-of-endpoints that could be considered for an exposure assessment study using 3-D organotypic nasal cultures: first, a cytotoxicity assay that is complemented by a morphological assessment (histology evaluation), second, a cellular molecular analysis leveraging a panel of genes playing a role in various biological processes (e.g. stress response, inflammatory response, apoptosis, and cell metabolism). Based on the present transcriptomics dataset, we have identified a reduced collection genes, which could be leveraged for qPCR analyses, comprising highly responsive genes altered upon smoke/aerosol exposure (Supplementary Fig. 6, http://dx.doi.org/10.14573/altex.1605041s). Those genes could be utilized for other studies with a reduced design, i.e. a small scale study involving only three exposure replicates. Furthermore, a selection of exposure-related endpoints could be used to build appropriate Adverse Outcome Pathways (AOPs). Such AOPs can correlate mechanistic data with the *in vivo* clinical endpoints of regulatory interest (Manuppello and Sullivan, 2015). To gain regulatory acceptance of any *in vitro* airway model system for predicting inhalation toxicity, *in vitro* airway model systems should be developed based on appropriate region-specific cells (BéruBé et al., 2009). Therefore, our systems toxicological assessment approach using a human *in vitro* 3-D nasal model will further support studies that enhance

insights into the molecular biology mechanisms associated with the impact of exposure to CS and candidate modified risk tobacco products, on the nasopharyngeal cavity of the human respiratory system.

References

Ackermann, M. and Strimmer, K. (2009). A general modular framework for gene set enrichment analysis. *BMC Bioinformatics 10*, 47. http://dx.doi.org/10.1186/1471-2105-10-47

Affymetrix miRNA QCT Tool (2011). Affymetrix miRNA QCTool: User's Guide. Available at: //media.affymetrix.com/support/downloads/manuals/mirna_qctool_user_manual.pdf.

Balls, M. (2010). ATLA (Alternatives to Laboratory Animals): past, present and future. *Altern Lab Anim 38*, 437-441. http://dx.doi.org/10.1038/laban0412-108

Baulig, A., Garlatti, M., Bonvallot, V. et al. (2003). Involvement of reactive oxygen species in the metabolic pathways triggered by diesel exhaust particles in human airway epithelial cells. *Am J Physiol Lung Cell Mol Physiol 285*, L671-679. http://dx.doi.org/10.1152/ajplung.00419.2002

Benjamini, Y. and Hochberg, Y. (1995). Controlling the False Discovery Rate: A Practical and Powerful Approach to Multiple Testing. *J R Stat Soc Series B Stat Methodol 57*, 289-300. http://dx.doi.org/10.2307/2346101

Berg, N., De Wever, B., Fuchs, H. W. et al. (2011). Toxicology in the 21st century--working our way towards a visionary reality. *Toxicol In Vitro 25*, 874-881. http://dx.doi.org/10.1016/j.tiv.2011.02.008

BéruBé, K., Aufderheide, M., Breheny, D. et al. (2009). In vitro models of inhalation toxicity and disease. *Altern Lab Anim 37*, 89-141.

Bolstad, B., Collin, F., Brettschneider, J. et al. (2005). Quality assessment of Affymetrix GeneChip data. In (eds.), *Bioinformatics and computational biology solutions using R and bioconductor*. Springer:Heidelberg.

Bolstad, B. M., Irizarry, R. A., Astrand, M. et al. (2003). A comparison of normalization methods for high density oligonucleotide array data based on variance and bias. *Bioinformatics 19*, 185-193.

Boué, S., Talikka, M., Westra, J. W. et al. (2015). Causal biological network database: a comprehensive platform of causal biological network models focused on the pulmonary and vascular systems. *Database 2015*, http://dx.doi.org/10.1093/database/bav030

Brekman, A., Walters, M. S., Tilley, A. E. et al. (2014). FOXJ1 Prevents Cilia Growth Inhibition by Cigarette Smoke in Human Airway Epithelium In Vitro. *Am J Respir Cell Mol Biol 51*, 688-700. http://dx.doi.org/10.1165/rcmb.2013-0363OC

Calderón-Garcidueñas, L., Rodriguez-Alcaraz, A., Garcia, R. et al. (1999). Cell proliferation in nasal respiratory epithelium of people exposed to urban pollution. *Carcinogenesis 20*, 383-389. http://dx.doi.org/10.1093/carcin/20.3.383

Carvalho, B. S. and Irizarry, R. A. (2010). A framework for oligonucleotide microarray preprocessing. *Bioinformatics 26*, 2363-2367. http://dx.doi.org/10.1093/bioinformatics/btq431

Chen, E. Y., Tan, C. M., Kou, Y. et al. (2013). Enrichr: interactive and collaborative HTML5 gene list enrichment analysis tool. *BMC Bioinformatics 14*, 128. http://dx.doi.org/10.1186/1471-2105-14-128

Chen, P., McGuire, J. K., Hackman, R. C. et al. (2008). Tissue Inhibitor of Metalloproteinase-1 Moderates Airway Re-Epithelialization by Regulating Matrilysin Activity. *Am J Pathol 172*, 1256-1270. http://dx.doi.org/10.2353/ajpath.2008.070891

Cohen, L., E, X., Tarsi, J. et al. (2007). Epithelial Cell Proliferation Contributes to Airway Remodeling in Severe Asthma. *Am J Respir Crit Care Med 176*, 138-145. http://dx.doi.org/10.1164/rccm.200607-1062OC

Cohen, N. A., Zhang, S., Sharp, D. B. et al. (2009). Cigarette smoke condensate inhibits transepithelial chloride transport and ciliary beat frequency. *Laryngoscope 119*, 2269-2274. http://dx.doi.org/10.1002/lary.20223

Constant, S., Wiszniewski, L. and Huang, S. (2014). *The Use of in vitro 3D Cell Models of Human Airway Epithelia (MucilAirTM) in Inhalation Toxicity. In Cellular In Vitro Testing: Methods and Protocols (Haycock, J., Whluwalia, A., and Wilkinson, M., Eds.), pp. 15-33. CRC Press, London, UK.* Vol. CRC Press.

d'Errico, A., Zajacova, J., Cacciatore, A. et al. (2013). Occupational risk factors for sinonasal inverted papilloma: a case-control study. *Occup Environ Med 70*, 703-708. http://dx.doi.org/10.1136/oemed-2013-101384

Dai, M., Wang, P., Boyd, A. D. et al. (2005). Evolving gene/transcript definitions significantly alter the interpretation of GeneChip data. *Nucleic Acids Res 33*, e175. http://dx.doi.org/10.1093/nar/gni179

Davis, M. A., Eldridge, S. and Louden, C. (2013). Chapter 10 - Biomarkers: Discovery, Qualification and Application. In W. M. H. G. R. A. Wallig (eds.), *Haschek and Rousseaux's Handbook of Toxicologic Pathology (Third Edition)*. Boston: Academic Press. http://www.sciencedirect.com/science/article/pii/B9780124157590000108 http://dx.doi.org/http://dx.doi.org/10.1016/B978-0-12-415759-0.00010-8

Dimova, S., Brewster, M., Noppe, M. et al. (2005). The use of human nasal in vitro cell systems during drug discovery and development. *Toxicol In Vitro 19*, 107-122. http://dx.doi.org/10.1016/j.tiv.2004.07.003

Ding, G. Q. and Zheng, C. Q. (2007). The expression of MUC5AC and MUC5B mucin genes in the mucosa of chronic rhinosinusitis and nasal polyposis. *Am J Rhinol 21*, 359-366. http://dx.doi.org/10.2500/ajr.2007.21.3037

Doke, S. K. and Dhawale, S. C. (2015). Alternatives to animal testing: A review. *Saudi Pharm J 23*, 223-229. http://dx.doi.org/10.1016/j.jsps.2013.11.002

Gautier, L., Cope, L., Bolstad, B. M. et al. (2004). affy--analysis of Affymetrix GeneChip data at the probe level. *Bioinformatics 20*, 307-315. http://dx.doi.org/10.1093/bioinformatics/btg405

Gonzalez-Suarez, I., Martin, F., Marescotti, D. et al. (2016). In Vitro Systems Toxicology Assessment of a Candidate Modified Risk Tobacco Product Shows Reduced Toxicity Compared to That of a Conventional Cigarette. *Chem Res Toxicol 29*, 3-18. http://dx.doi.org/10.1021/acs.chemrestox.5b00321

Harkema, J. R., Carey, S. A. and Wagner, J. G. (2006). The nose revisited: a brief review of the comparative structure, function, and toxicologic pathology of the nasal epithelium. *Toxicol Pathol 34*, 252-269. http://dx.doi.org/10.1080/01926230600713475

Health Canada (1999). Determination of Tar, Water, Nicotine and Carbon Monoxide in Mainstream Tobacco Smoke. Health Canada Test Method T-11.

Hoeng, J., Talikka, M., Martin, F. et al. (2014). Case study: the role of mechanistic network models in systems toxicology. *Drug Discov Today 19*, 183-192. http://dx.doi.org/10.1016/j.drudis.2013.07.023

Huber, W., Carey, V. J., Gentleman, R. et al. (2015). Orchestrating high-throughput genomic analysis with Bioconductor. *Nat Methods 12*, 115-121. http://dx.doi.org/10.1038/nmeth.3252

Hukkanen, J., Pelkonen, O., Hakkola, J. et al. (2002). Expression and regulation of xenobiotic-metabolizing cytochrome P450 (CYP) enzymes in human lung. *Crit Rev Toxicol 32*, 391-411. http://dx.doi.org/10.1080/20024091064273

Hussain, T., Al-Attas, O. S., Al-Daghri, N. M. et al. (2014). Induction of CYP1A1, CYP1A2, CYP1B1, increased oxidative stress and inflammation in the lung and liver tissues of rats exposed to incense smoke. *Mol Cell Biochem 391*, 127-136. http://dx.doi.org/10.1007/s11010-014-1995-5

Huvenne, W., Pérez-Novo, C. A., Derycke, L. et al. (2010). Different regulation of cigarette smoke induced inflammation in upper versus lower airways. *Respir Res 11*, 100. http://dx.doi.org/10.1186/1465-9921-11-100

International Organization for Standardization ISO 3402: 1999Tobacco and tobacco products -- Atmosphere for conditioning and testing. Available at: http://www.iso.org/iso/home/store/catalogue_tc/catalogue_detail.htm?csnumber=28324.

Iskandar, A. R., Xiang, Y., Frentzel, S. et al. (2015). Impact Assessment of Cigarette Smoke Exposure on Organotypic Bronchial Epithelial Tissue Cultures: A Comparison of Mono-Culture and Coculture Model Containing Fibroblasts. *Toxicol Sci 147*, 207-221. http://dx.doi.org/10.1093/toxsci/kfv122

Kanehisa, M., Goto, S., Sato, Y. et al. (2014). Data, information, knowledge and principle: back to metabolism in KEGG. *Nucleic Acids Res 42*, D199-205. http://dx.doi.org/10.1093/nar/gkt1076

Kauffmann, A., Gentleman, R. and Huber, W. (2009). arrayQualityMetrics--a bioconductor package for quality assessment of microarray data. *Bioinformatics 25*, 415-416. http://dx.doi.org/10.1093/bioinformatics/btn647

Kim, D.-D. (2008). In vitro cellular models for nasal drug absorption studies. In (eds.), *Drug Absorption Studies*. Springer. http://dx.doi.org/10.1007/978-0-387-74901-3

Kozomara, A. and Griffiths-Jones, S. (2013). miRBase: annotating high confidence microRNAs using deep sequencing data. *Nucleic Acids Research* http://dx.doi.org/10.1093/nar/gkt1181

Kreindler, J. L., Jackson, A. D., Kemp, P. A. et al. (2005). Inhibition of chloride secretion in human bronchial epithelial cells by cigarette smoke extract. *Am J Physiol Lung Cell Mol Physiol 288*, L894-902. http://dx.doi.org/10.1152/ajplung.00376.2004

Krewski, D., Acosta, D., Andersen, M. et al. (2010). Toxicity Testing in the 21st Century: a Vision and a Strategy. *J Toxicol Environ Health B Crit Rev 13*, 51-138. http://dx.doi.org/10.1080/10937404.2010.483176

Kuper, H., Boffetta, P. and Adami, H. O. (2002). Tobacco use and cancer causation: association by tumour type. *J Intern Med 252*, 206-224.

Lan, M.-Y., Ho, C.-Y., Lee, T.-C. et al. (2007). Cigarette smoke extract induces cytotoxicity on human nasal epithelial cells. *Am J Rhinol Allergy 21*, 218-223. http://dx.doi.org/10.2500/ajr.2007.21.2966

Lee, H. S. and Kim, J. (2013). Cigarette smoke inhibits nasal airway epithelial cell growth and survival. Int Forum Allergy Rhinol, *Wiley Online Library 3*, 188-192. http://dx.doi.org/10.1002/alr.21129

Leopold, P. L., O'Mahony, M. J., Lian, X. J. et al. (2009). Smoking is associated with shortened airway cilia. *PLoS One 4*, e8157. http://dx.doi.org/10.1371/journal.pone.0008157

Majeed, S., Frentzel, S., Wagner, S. et al. (2014). Characterization of the Vitrocell® 24/48 in vitro aerosol exposure system using mainstream cigarette smoke. *Chem Cent J 8*, 1-11. http://dx.doi.org/10.1186/s13065-014-0062-3

Manuppello, J. R. and Sullivan, K. M. (2015). Toxicity assessment of tobacco products in vitro. *Altern Lab Anim 43*, 39-67.

Martin, F., Thomson, T., Sewer, A. et al. (2012). Assessment of network perturbation amplitudes by applying high-throughput data to causal biological networks. *BMC Systems Biology 6*, 54. http://dx.doi.org/10.1186/1752-0509-6-54

Martin, F., Sewer, A., Talikka, M. et al. (2014). Quantification of biological network perturbations for mechanistic insight and diagnostics using two-layer causal models. *BMC Bioinformatics 15*, 238. http://dx.doi.org/10.1186/1471-2105-15-238

Marwick, J. A., Stevenson, C. S., Giddings, J. et al. (2006). Cigarette smoke disrupts VEGF165-VEGFR-2 receptor signaling complex in rat lungs and patients with COPD: morphological impact of VEGFR-2 inhibition. *Am J Physiol Lung Cell Mol Physiol 290*, L897-L908. http://dx.doi.org/10.1152/ajplung.00116.2005

Mathis, C., Poussin, C., Weisensee, D. et al. (2013). Human bronchial epithelial cells exposed in vitro to cigarette smoke at the air-liquid interface resemble bronchial epithelium from human smokers. *Am J Physiol Lung Cell Mol Physiol 304*, L489-503. http://dx.doi.org/10.1152/ajplung.00181.2012

McCall, M. N., Bolstad, B. M. and Irizarry, R. A. (2010). Frozen robust multiarray analysis (fRMA). *Biostatistics 11*, 242-253. http://dx.doi.org/10.1093/biostatistics/kxp059

Mestdagh, P., Van Vlierberghe, P., De Weer, A. et al. (2009). A novel and universal method for microRNA RT-qPCR data normalization. *Genome Biology 10*, 1-10. http://dx.doi.org/10.1186/gb-2009-10-6-r64

Moon, I. J., Lee, D. Y., Suh, M. W. et al. (2010). Cigarette smoking increases risk of recurrence for sinonasal inverted papilloma. *Am J Rhinol Allergy 24*, 325-329. http://dx.doi.org/10.2500/ajra.2010.24.3510

Peppercorn, J. (2013). Toward Improved Understanding of the Ethical and Clinical Issues Surrounding Mandatory Research Biopsies. *J Clin Oncol 31*, 1-2. http://dx.doi.org/10.1200/jco.2012.44.8589

Phillips, B., Veljkovic, E., Boué, S. et al. (2016). An 8-Month Systems Toxicology Inhalation/Cessation Study in Apoe(−/−) Mice to Investigate Cardiovascular and Respiratory Exposure Effects of a Candidate Modified Risk Tobacco Product, THS 2.2, Compared With Conventional Cigarettes. *Toxicol Sci 149*, 411-432. http://dx.doi.org/10.1093/toxsci/kfv243

Pritchard, C. C., Cheng, H. H. and Tewari, M. (2012). MicroRNA profiling: approaches and considerations. *Nat Rev Genet 13*, 358-369. http://dx.doi.org/http://www.nature.com/nrg/journal/v13/n5/suppinfo/nrg3198_S1.html

R Core Team (2013). R: A language and environment for statistical computing. R Foundation for Statistical Computing, Vienna, Austria. Available at: http://www.R-project.org/.

Ritchie, M. E., Phipson, B., Wu, D. et al. (2015). limma powers differential expression analyses for RNA-sequencing and microarray studies. *Nucleic Acids Research* http://dx.doi.org/10.1093/nar/gkv007

Rovida, C., Asakura, S., Daneshian, M. et al. (2015). Toxicity testing in the 21st century beyond environmental chemicals. *ALTEX 32*, 171-181. http://dx.doi.org/http://dx.doi.org/10.14573/altex.1506201

Sales, G., Calura, E., Cavalieri, D. et al. (2012). graphite - a Bioconductor package to convert pathway topology to gene network. *BMC Bioinformatics 13*, 20. http://dx.doi.org/10.1186/1471-2105-13-20

Sham, C. L., Lee, D. L., van Hasselt, C. A. et al. (2010). A case-control study of the risk factors associated with sinonasal inverted papilloma. *Am J Rhinol Allergy 24*, e37-40. http://dx.doi.org/10.2500/ajra.2010.24.3408

Sheldon, L. S. and Cohen Hubal, E. A. (2009). Exposure as part of a systems approach for assessing risk. *Environ Health Perspect 117*, 119-1194. http://dx.doi.org/10.1289/ehp.0800407

Smith, C., Djakow, J., Free, R. et al. (2012). ciliaFA: a research tool for automated, high-throughput measurement of ciliary beat frequency using freely available software. *Cilia 1*, 14. http://dx.doi.org/10.1186/2046-2530-1-14

Smyth, G. K. (2004). Linear models and empirical bayes methods for assessing differential expression in microarray experiments. *Stat Appl Genet Mol Biol 3*, Article3. http://dx.doi.org/10.2202/1544-6115.1027

Sridhar, S., Schembri, F., Zeskind, J. et al. (2008). Smoking-induced gene expression changes in the bronchial airway are reflected in nasal and buccal epithelium. *BMC genomics 9*, 259. http://dx.doi.org/10.1186/1471-2164-9-259

Stanley, P. J., Wilson, R., Greenstone, M. A. et al. (1986). Effect of cigarette smoking on nasal mucociliary clearance and ciliary beat frequency. *Thorax 41*, 519-523. http://dx.doi.org/10.1136/thx.41.7.519

Szabo, E. (2001). Lung Epithelial Proliferation: a Biomarker for Chemoprevention Trials? *J Natl Cancer Inst 93*, 1042-1043. http://dx.doi.org/10.1093/jnci/djm221

t Mannetje, A., Kogevinas, M., Luce, D. et al. (1999). Sinonasal cancer, occupation, and tobacco smoking in European women and men. *Am J Ind Med 36*, 101-107. http://dx.doi.org/10.1002/(SICI)1097-0274(199907)36:1<101::AID-AJIM14>3.0.CO;2-A

Talikka, M., Kostadinova, R., Xiang, Y. et al. (2014). The response of human nasal and bronchial organotypic tissue cultures to repeated whole cigarette smoke exposure. *Int J Toxicol 33*, 506-517. http://dx.doi.org/10.1177/1091581814551647

Varemo, L., Nielsen, J. and Nookaew, I. (2013). Enriching the gene set analysis of genome-wide data by incorporating directionality of gene expression and combining statistical hypotheses and methods. *Nucleic Acids Res 41*, 4378-4391. http://dx.doi.org/10.1093/nar/gkt111

Virgin, F. W., Azbell, C., Schuster, D. et al. (2010). Exposure to Cigarette Smoke Condensate Reduces Calcium Activated Chloride Channel Transport in Primary Sinonasal Epithelial Cultures. *Laryngoscope 120*, 1465-1469. http://dx.doi.org/10.1002/lary.20930

Vlachos, I. S., Paraskevopoulou, M. D., Karagkouni, D. et al. (2015). DIANA-TarBase v7.0: indexing more than half a million experimentally supported miRNA:mRNA interactions. *Nucleic Acids Res 43*, D153-159. http://dx.doi.org/10.1093/nar/gku1215

Yu, M. S., Park, H. W., Kwon, H. J. et al. (2011). The effect of a low concentration of hypochlorous acid on rhinovirus infection of nasal epithelial cells. *Am J Rhinol Allergy 25*, 40-44. http://dx.doi.org/10.2500/ajra.2011.25.3545

Acknowledgements

The authors would like to thank Walter Schlage for his critical review of the manuscript. The authors also acknowledge Grégory Vuillaume and Gilles Kreutzer for statistical evaluation support. We also thank the following individuals for contributing their technical expertise: Laura Ortega Torres and Stephanie Johne (handling of nasal cultures and measurements of cytotoxicity, CYP activity, and cilia beating); Abdelkader Benyagoub, Camille Schilt and Maude Mayer (histological processing); Flavia Buchler and Maica Corciulo (support of Luminex-based measurement); and Karine Baumer, Dariusz Peric (RNA purification); as well as Remi Dulize and Sophie Scheuner (microarray experiments). Part of the data was presented at the 9th World Congress in Prague (Cabanski, M. et al. (2014), *ALTEX Proceedings 3* (1); 36) and Society of Toxicology Annual Meeting in New Orleans, LA, USA (Iskandar, A.R. et al. (2016), Abstract no. 3036).

Conflict of Interest Statements

All authors are employees of Philip Morris International. Philip Morris International is the sole source of funding and sponsor of this project.

ALTEX Online first
published July 7, 2016
http://dx.doi.org/10.14573/altex.1605041

Correspondence to
Anita R. Iskandar, PhD
Biological Systems Research
Philip Morris International R&D
Quai Jeanrenaud 5
CH-2000 Neuchatel
Switzerland
Phone: +41 58 242 2777
Email: anita.iskandar@pmi.com

ALTEX Online first
published July 7, 2016
http://dx.doi.org/10.14573/altex.1605041

Figure 1

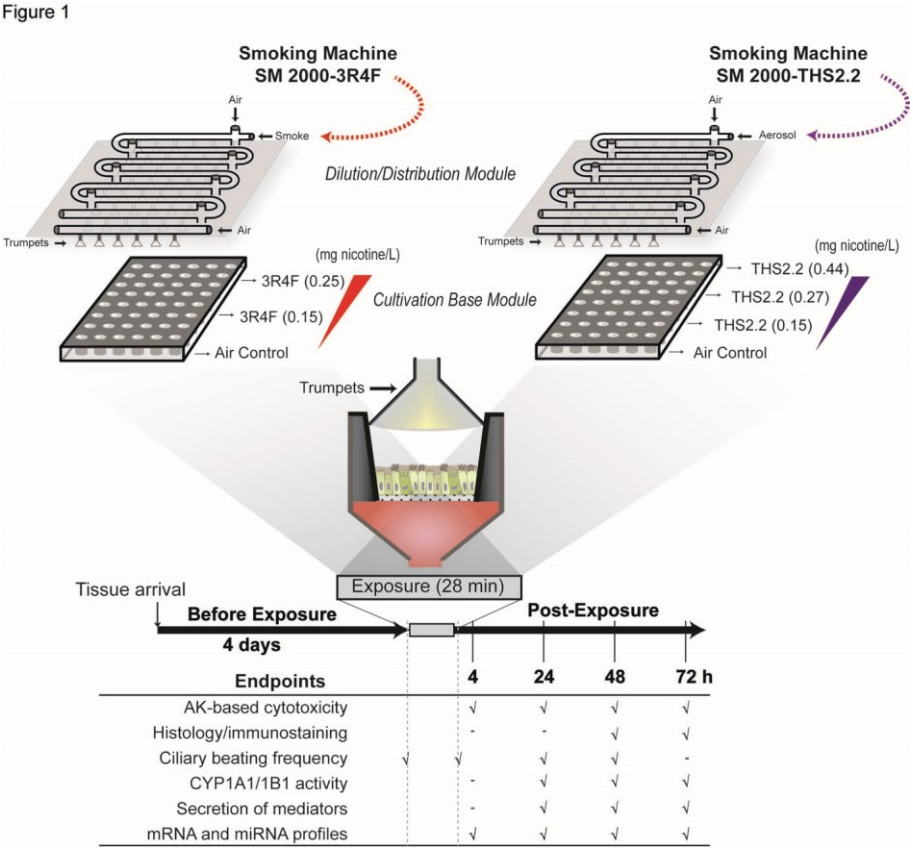


Fig. 1: Experimental design
During a given exposure run, 3-D nasal cultures were exposed to 3R4F smoke or THS2.2 aerosol from their apical side. Two independent Vitrocell® 24/48 exposure systems were used: a 3R4F smoke exposure run was performed by connecting the exposure system to the smoking machine (SM) 2000-3R4F, and THS2.2 aerosol exposure was performed by connecting the system to SM 2000-THS2.2. Specific dilutions within the Dilution/Distribution Module of the Vitrocell® 24/48 exposure system were applied to reach target nicotine concentrations (mg nicotine/L 3R4F smoke or mg nicotine/L THS2.2 aerosol) through individual trumpets to each well. For each group, a collection of endpoints was measured at different post-exposure time points (the total sample number per endpoints obtained throughout the study is given in Fehler! Verweisquelle konnte nicht gefunden werden.).

ALTEX Online first
published July 7, 2016
http://dx.doi.org/10.14573/altex.1605041

Figure 2

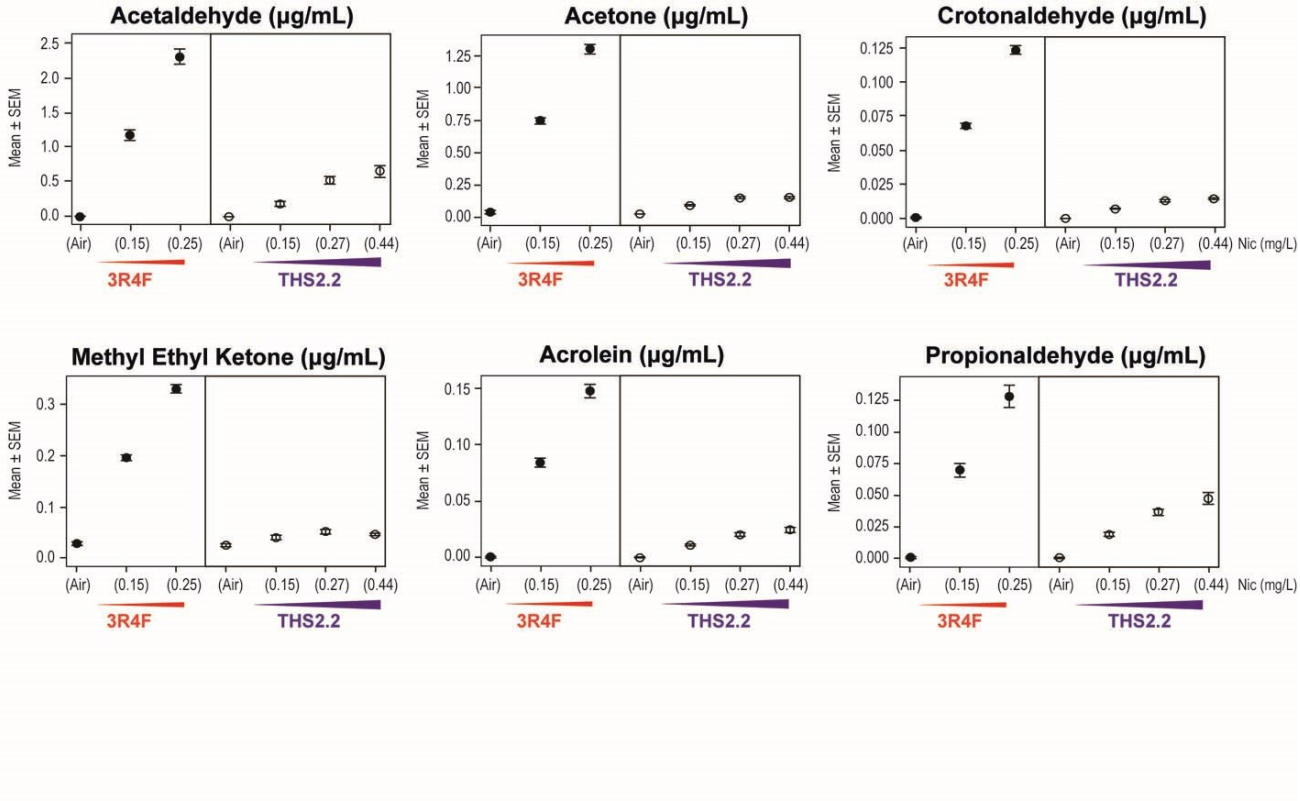


Fig. 2: Deposited concentrations of carbonyls in the Vitrocell® Base Module following 3R4F smoke and THS2.2 aerosol exposure

The mean of the representative carbonyls deposited in the PBS-filled Vitrocell® Base Module after a 28 min 3R4F smoke and THS2.2 aerosol exposure at the applied concentrations are shown. 3R4F smoke concentrations were applied at 0.15 and 0.25 mg nicotine/L smoke. Whereas THS2.2 aerosol concentrations were applied at 0.15, 0.27, and 0.44 mg nicotine/L aerosol. The concentration of carbonyls is reported as µg/mL PBS. Abbreviations: N, number of samples; SEM, standard error mean.

ALTEX Online first
published July 7, 2016
http://dx.doi.org/10.14573/altex.1605041

Figure 3

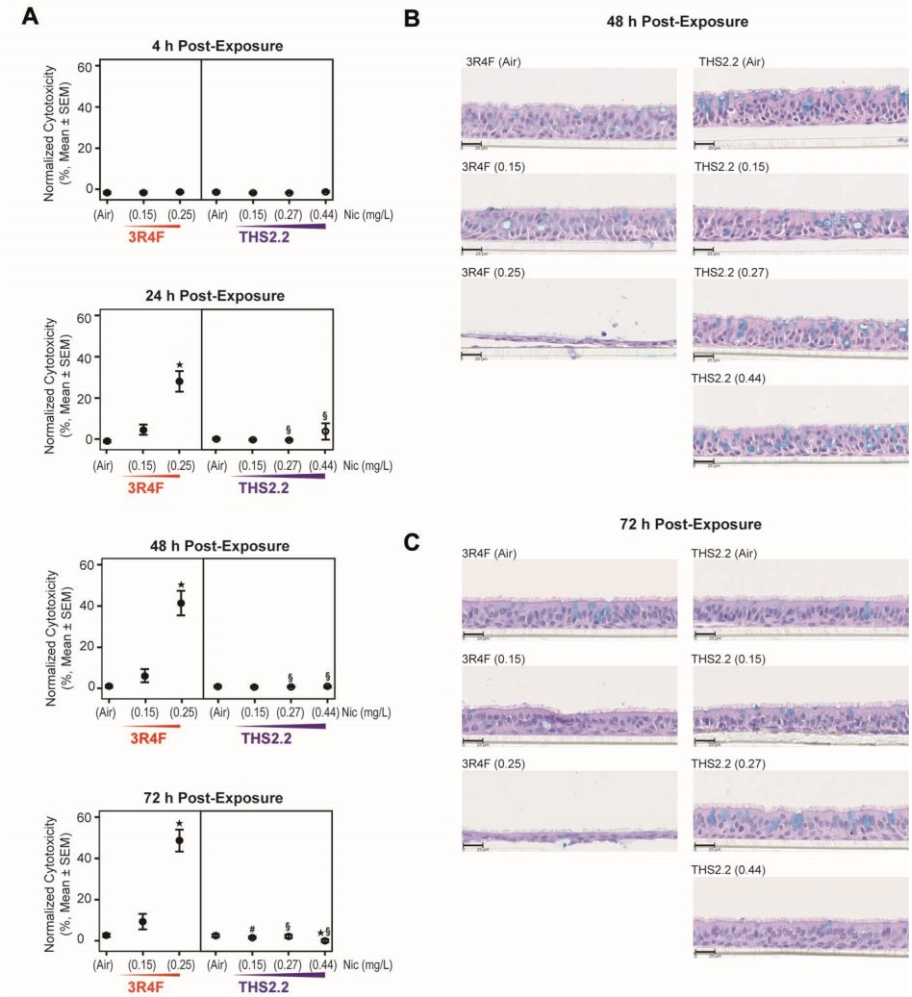


Fig. 3: Cytotoxicity and tissue morphology after exposure
(A) Mean cytotoxicity levels evaluated by AK assay at various time points post-exposure. The AK levels were normalized relative to the positive and negative controls (see Materials and Methods). Nicotine concentrations in 3R4F smoke or THS2.2 aerosols are indicated for each group (mg/L, x-axis). ★ indicates $p < 0.05$ compared with their corresponding air controls. # indicates $p < 0.05$ differences with 3R4F (0.15) and § indicates the difference with 3R4F (0.25). (B) and (C) Representative images of H&E/Alcian Blue-stained nasal culture sections observed at 48 and 72 h post-exposure, respectively. Abbreviations: AK, adenylate kinase; H&E, hematoxylin and eosin; SEM, standard error mean.

ALTEX Online first
published July 7, 2016
http://dx.doi.org/10.14573/altex.1605041

Figure 4

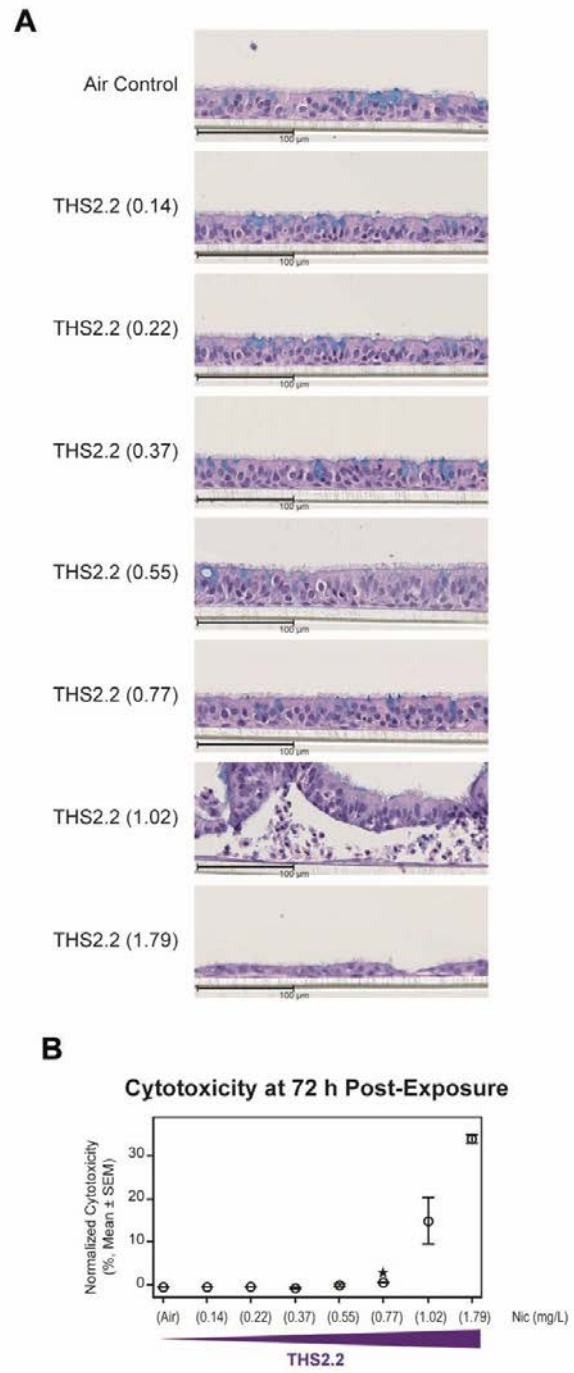


Fig. 4: Dose range assessment of THS2.2 aerosol
(A) H&E-stained tissue sections at 72 h post-exposure. Number in parentheses indicate the concentration of nicotine in the THS2.2 aerosol (mg/L). The experimental procedure of the exposure run is reported in Fehler! Verweisquelle konnte nicht gefunden werden.. (B) Mean cytotoxicity levels at 72 h post-exposure, determined by AK assay, normalized to those of the positive control (Triton X-100 treated samples). ★ indicates $p < 0.05$ compared with the air control. Abbreviations: AK, adenylate kinase; H&E, hematoxylin and eosin; SEM, standard error mean.

ALTEX Online first
published July 7, 2016
http://dx.doi.org/10.14573/altex.1605041

Figure 5

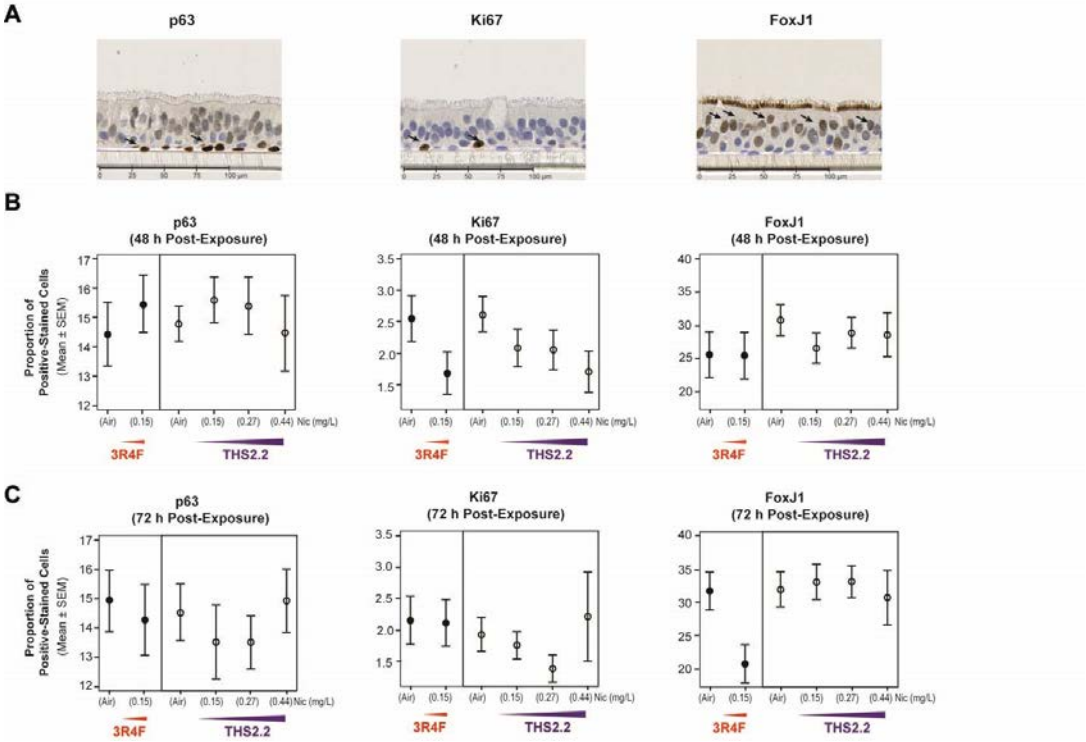


Fig. 5: Quantification of p63, Ki67, and FoxJ1 immunostaining
(A) Representative images of the immunostained nasal culture sections. Arrows indicate the representative positive-stained cells. (B) and (C) Mean proportions of positive-stained cells in the sections of 3R4F-exposed and THS2.2-exposed cultures assessed at 48 and 72 h post-exposure, respectively. The proportion of positively-stained cells was digitally quantified relative to the total cell number. Nicotine concentrations in 3R4F smoke or THS2.2 aerosols are indicated for each group (mg/L, x-axis). Abbreviations: SEM, standard error mean.

ALTEX Online first
published July 7, 2016
http://dx.doi.org/10.14573/altex.1605041

Figure 6

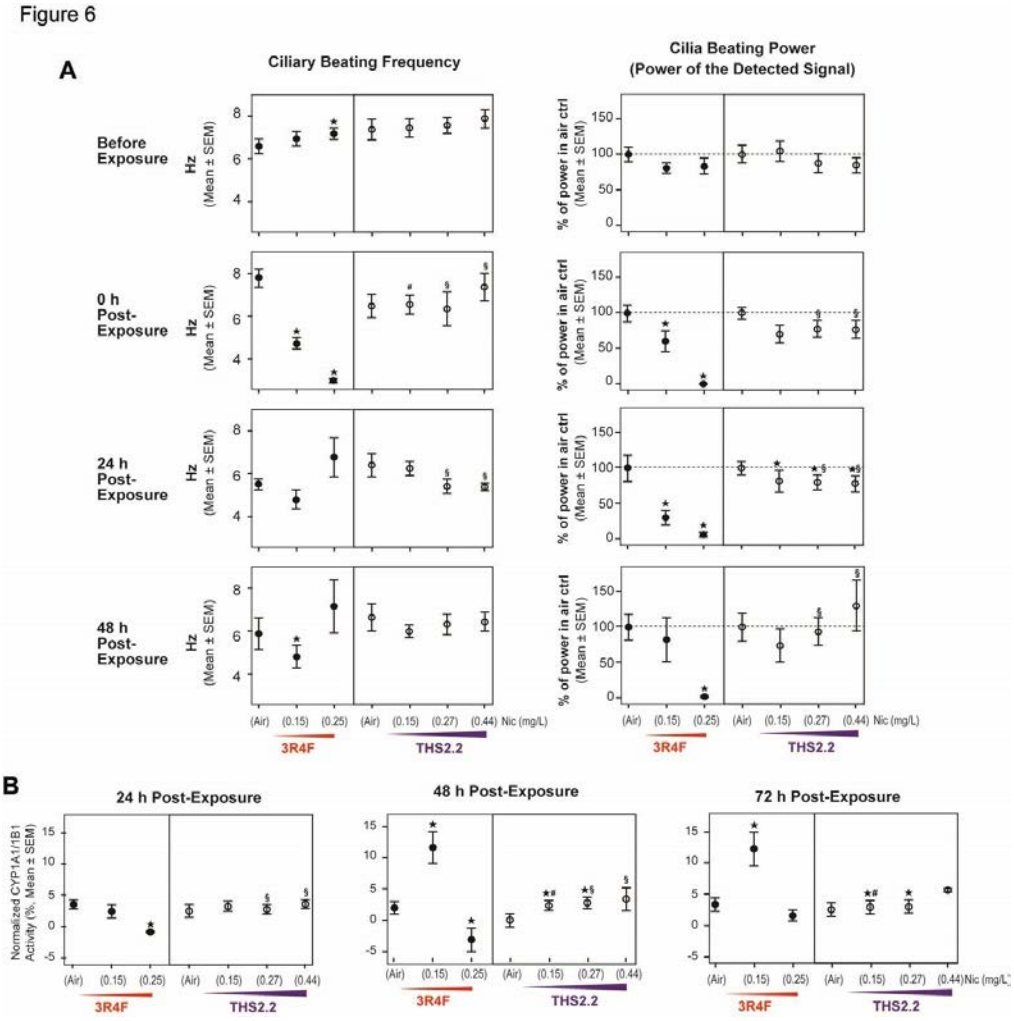


Fig. 6: Alterations of cilia beating frequency and activity of CYP1A1/CYP1B1
(A) Mean levels of cilia beating frequency (left panels) and the power magnitude of the detected beating signal (right panels) before exposure and at various time points after exposure. (B) Mean activity levels of CYP1A1/CYP1B1 (combined). The activity levels were normalized relative to the positive control (TCDD-treated cultures considered as 100% activity). Nicotine concentrations in the smoke or aerosol are indicated for each group (mg/L, x-axis). ★ indicates $p < 0.05$ compared with their corresponding air controls. # indicates $p < 0.05$ differences with 3R4F (0.15) and § indicates the difference with 3R4F (0.25). Abbreviations: CYP, cytochrome P450; SEM, standard error mean, TCDD, 2,3,7,8-Tetrachlorodibenzodioxin.

ALTEX Online first
published July 7, 2016
http://dx.doi.org/10.14573/altex.1605041

Figure 7

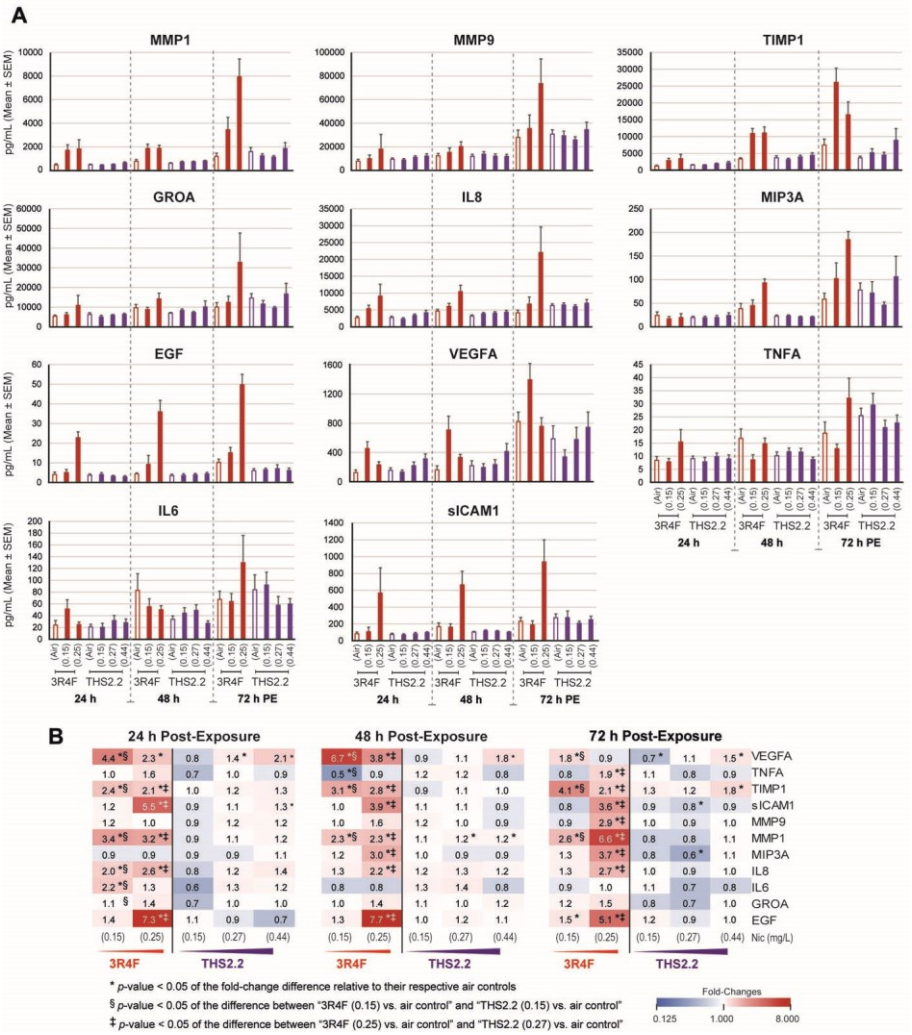


Fig. 7: Profiles of secreted pro-inflammatory mediators following exposure
(A) Mean concentrations of pro-inflammatory mediators measured in the basolateral media of the cultures at 24, 48, or 72 h post-exposure (PE) for each group. (B) Heatmaps showing the fold-changes of the mean concentrations relative to their corresponding air control. Red and blue represent the degree of increased and decreased fold-changes, respectively. Nicotine concentrations in the smoke or aerosol are indicated for each group (mg/L, x-axis).

ALTEX Online first
published July 7, 2016
http://dx.doi.org/10.14573/altex.1605041

Figure 8

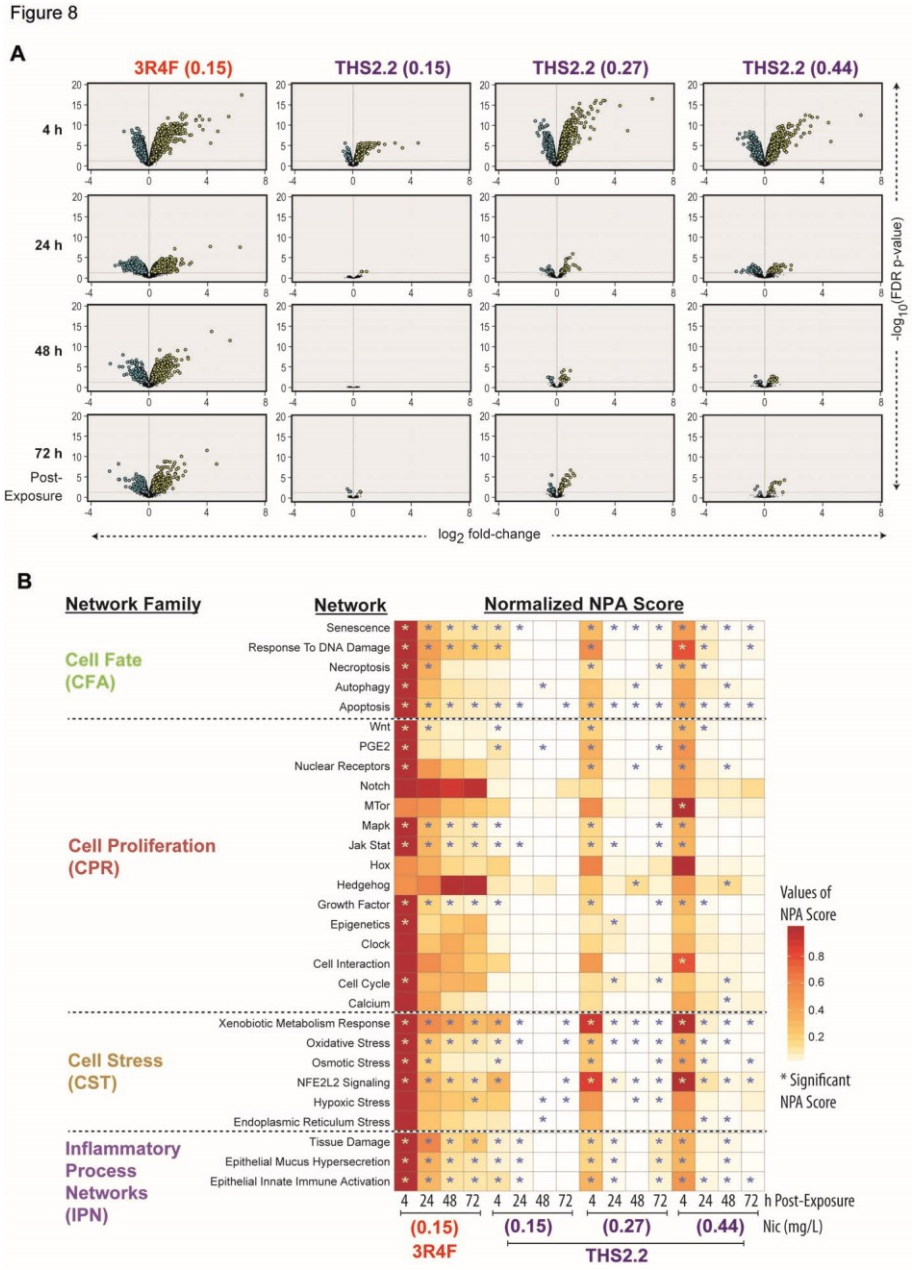


Fig. 8: Impact of exposure on the global gene expression and biological network models
(A) Volcano plots showing the alterations of gene expressions (each dot represents a gene) for each exposure group as compared with the air control. The changes of gene expression (x-axis) are shown as increased and decreased when > 0 and < 0, respectively. -$\log_{10}$ FDR p-value is displayed in the *y-axis*. A FDR *p*-value = 0.05 is considered as the statistical significance threshold. (B) Perturbation levels for various network models (exposed group vs. air control). The network names and their families are listed on the left side of the heatmap. The color gradient represents scores of the network perturbation (based on the NPA algorithm), which are normalized to the maximum NPA score per network. A network is considered significantly perturbed (*) if the NPA score remains significant after accounting for the experimental variation and if the companion statistics O and K are significant (*p*-values < 0.05, described in Materials and Methods).

ALTEX Online first
published July 7, 2016
http://dx.doi.org/10.14573/altex.1605041

Figure 9

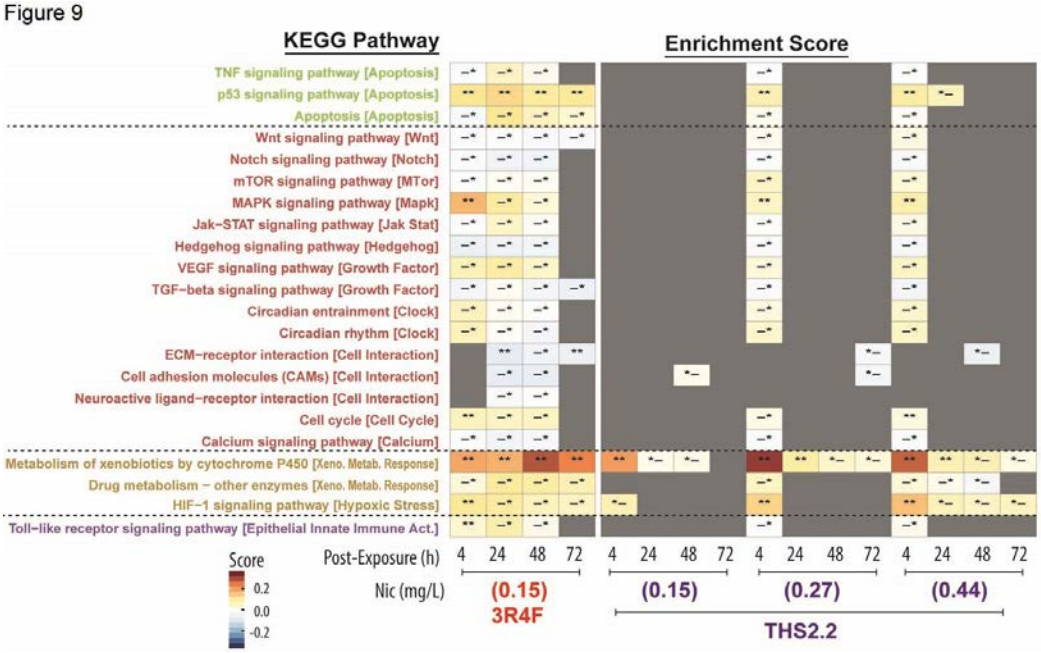


Fig. 9: Gene-set analysis showing various biological pathways enriched in the datasets
A heatmap showing selected KEGG pathways (those corresponding to the network models) that were significantly enriched in the dataset. The corresponding network models are designated using square brackets ([ ]). The color gradient represents the score enrichment: the mean of the gene score ($\log_2$(fold-change)). Gray color indicates a lack of pathway annotation in the respective datasets. Two categories of significance are shown: first and second characters indicate the Q1 and Q2, respectively (see Materials and Methods).

ALTEX Online first
published July 7, 2016
http://dx.doi.org/10.14573/altex.1605041

Figure 10

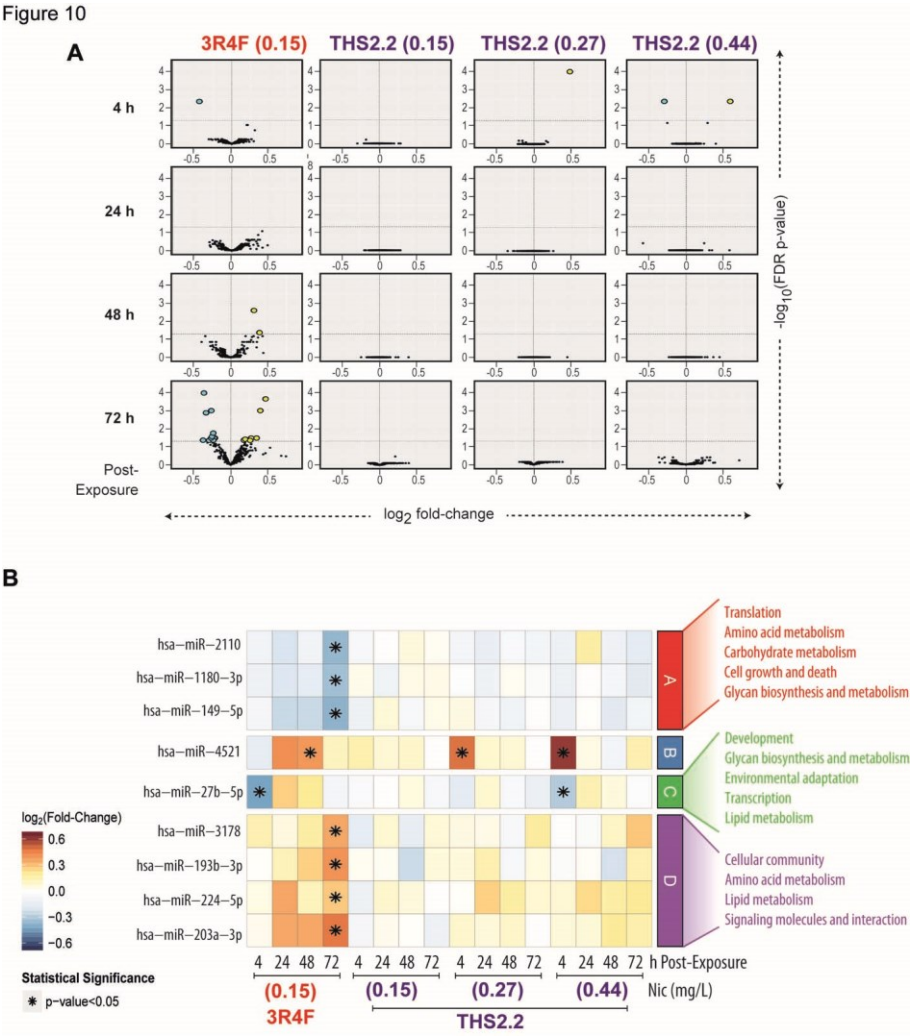


Fig. 10. Exposure impact on the global miRNA expression.
(A) Volcano plots showing alterations of miRNAs expression (each dot represents one miRNA) for each exposure group as compared with the air controls. Changes of miRNA expression (x-axis) are shown as increased and decreased when > 0 and < 0, respectively. The statistical significance is displayed in the y-axis (at FDR p-value < 0.05). (B) A heatmap showing miRNAs that are significantly altered, with fold-changes of at least 0.33 (*) in at least one contrast (exposed group vs. air control). The color gradient represents alterations of miRNA levels (log2(fold-change). Clusters a, b, c, and d represent changes in miRNA patterns linked to the annotation of various KEGG pathway classes, as described in the Material and Methods.

ALTEX Online first
published July 7, 2016
http://dx.doi.org/10.14573/altex.1605041

Figure 11

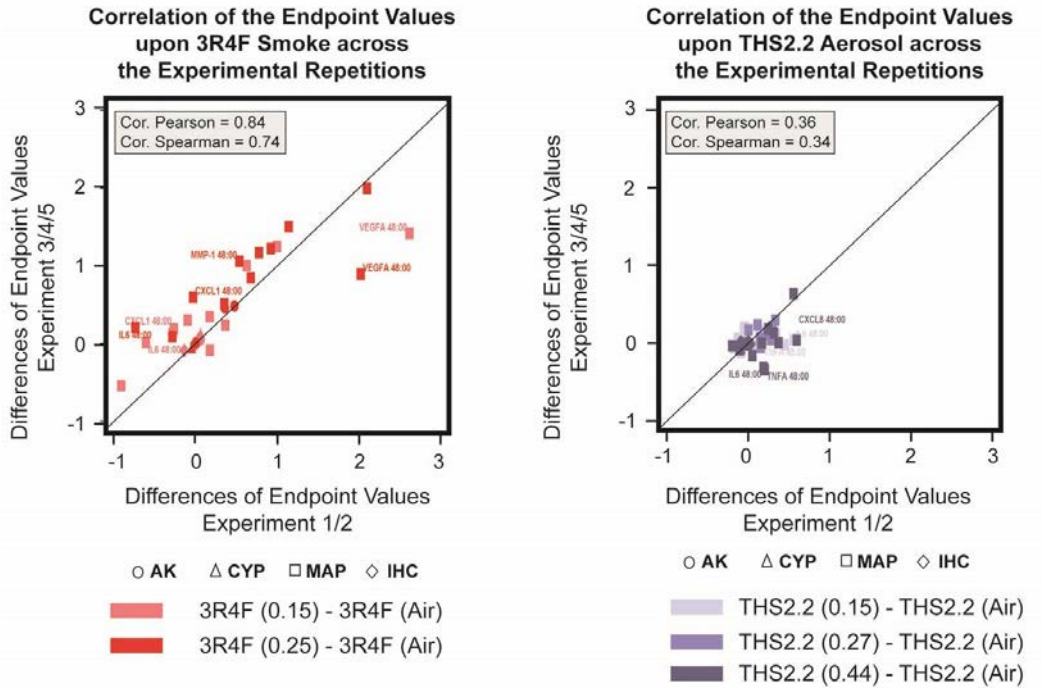


Fig. 11: Correlation plots of the observed values (functional cellular assays) obtained across the experimental repetitions

The mean of the differences of endpoint values (exposed vs. control), which were obtained from experimental repetition 1 and 2 (*x-axis*), were correlated to those obtained from experimental repetition 3, 4 and 5 (*y-axis*). Different symbols highlight the different endpoints: AK (the normalized cytotoxicity measurement), CYP (the normalized activity of CYP1A1/1B1), and MAP (the logarithm based 10 of the concentration measured using Luminex based analyses of pro-inflammatory mediators), as well as IHC (the proportion of the p63, Ki67, and FoxJ1 positive stained cells). A 45-degree line is drawn to aid the visualization. Data points farther away from the 45-degree line are labelled. A Spearman and Pearson correlations were computed. Abbreviations: AK, adenylate kinase; Cor, correlation; CYP, cytochrome P450; IHC, immunohistochemistry; MAP, multianalyte profiling.

Figure 12

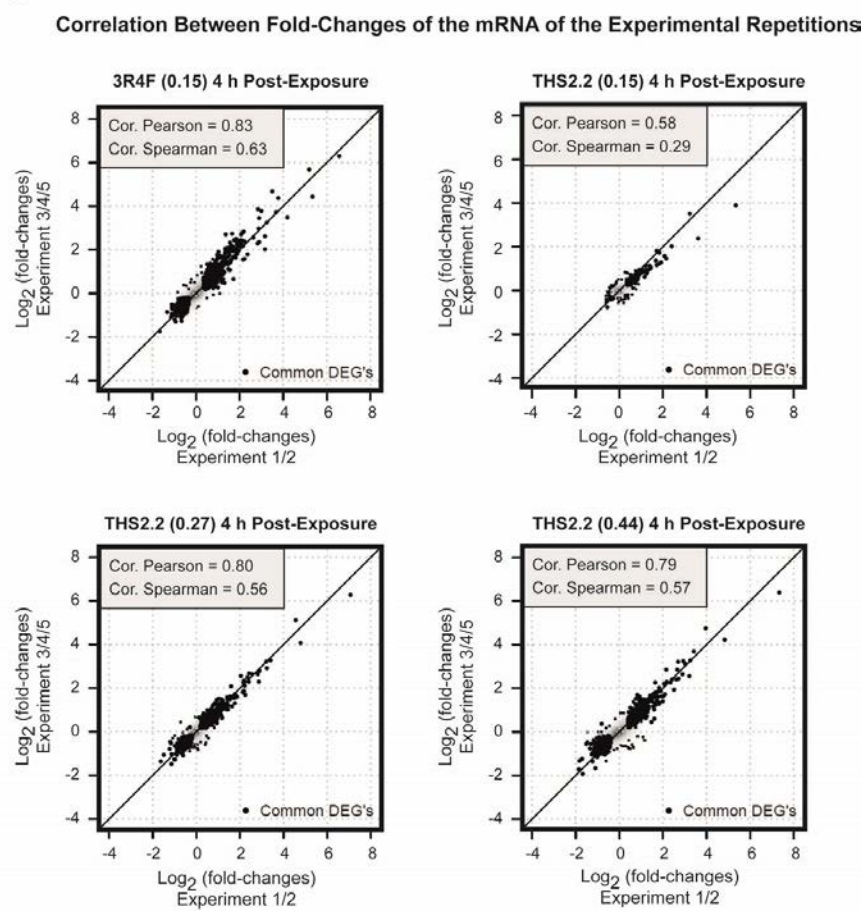


Fig. 12: Correlation plots of gene fold-changes generated from the array analysis.
Each dot represents a gene. The fold-change of a given gene from the combined experiments 1 and 2 (x-axis) was compared with the fold-change of the same gene from the combined experiment 3, 4, and 5 (y-axis). Abbreviations: Cor, correlation; DEG, differentially expressed gene. The correlation plots for all groups are reported in Fehler! Verweisquelle konnte nicht gefunden werden..

Figure 13

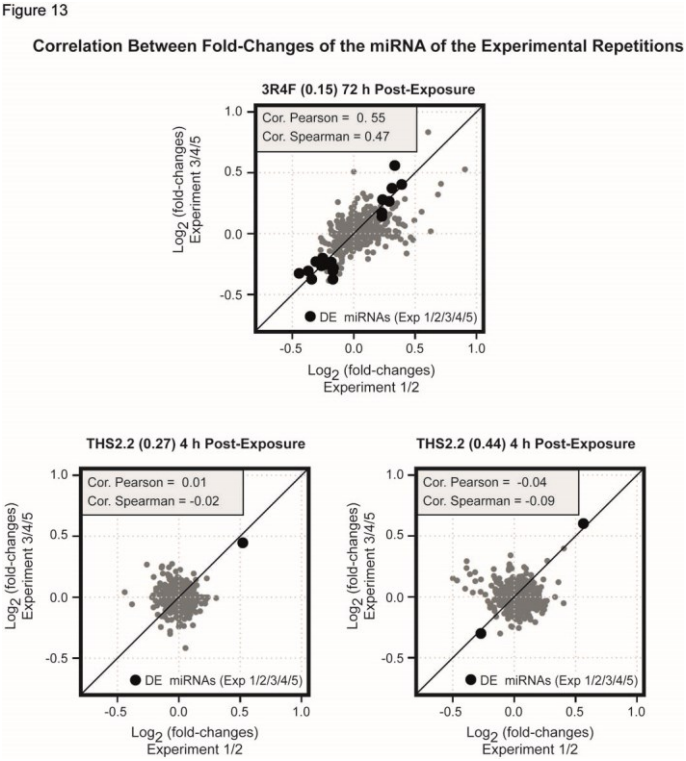


Fig. 13: Correlation plots of miRNA fold-changes generated from the array analysis
Each dot represents a miRNA. The fold-change of a given miRNA from combined experiments 1 and 2 (x-axis) was compared with the fold-change of the same gene from combined experiments 3, 4, and 5 (y-axis). Abbreviations: Cor, correlation; DE, differentially expressed. The comparability of the miRNA fold-changes obtained across the experimental repetitions are reported in Supplementary Fig. 5.

ALTEX Online first
published July 7, 2016
http://dx.doi.org/10.14573/altex.1605041

Tab. 1: Target and Actual Concentrations of Nicotine in the Diluted 3R4F Smoke and THS2.2 Aerosol

Group		Trapping 1	Trapping 2	Trapping 3	Trapping 4
3R4F Low Concentration	Target Nicotine (mg/L)	0.15	0.15	0.15	0.15
	Dilution in Vitrocell (%)	8.0	7.0	7.0	7.0
	Actual Nicotine (mg/L)	0.139 ± 0.005 (N = 3)	0.137 ± 0.007 (N = 3)	0.155 ± 0.004 (N = 3)	0.156 ± 0.007 (N = 3)
3R4F High Concentration	Target Nicotine (mg/L)	0.25	0.25	0.25	0.25
	Dilution in Vitrocell (%)	15.0	13.0	13.0	13.0
	Actual Nicotine (mg/L)	0.240 ± 0.013 (N = 4)	0.247 ± 0.06 (N = 3)	0.257 ± 0.004 (N = 3)	0.263 ± 0.011 (N = 3)
THS2.2 Low Concentration	Target Nicotine (mg/L)	0.15	0.15	0.15	0.15
	Dilution in Vitrocell (%)	12.8	13.0	13.0	13.0
	Actual Nicotine (mg/L)	0.145 ± 0.04 (N = 3)	0.148 ± 0.007 (N = 3)	0.144 ± 0.001 (N = 3)	0.154 ± 0.04 (N = 4)
THS2.2 Medium Concentration	Target Nicotine (mg/L)	0.27	0.27	0.27	0.27
	Dilution in Vitrocell (%)	22.6	24.0	24.0	24.0
	Actual Nicotine (mg/L)	0.260 ± 0.042 (N = 3)	0.279 ± 0.032 (N = 3)	0.292 ± 0.006 (N = 3)	0.266 ± 0.008 (N = 4)
THS2.2 High Concentration	Target Nicotine (mg/L)	0.44	0.44	0.44	0.44
	Dilution in Vitrocell (%)	31.0	31.0	31.0	31.0
	Actual Nicotine (mg/L)	0.413 ± 0.017 (N = 3)	0.437 ± 0.015 (N = 3)	0.439 ± 0.009 (N = 3)	0.452 ± 0.021 (N = 3)

The actual nicotine concentrations are expressed as the mean ± SEM. Abbreviations: N, number of samples (trapped in the EXtrelut® 3NT columns); NA, not available (the concentration was not tested in the experimental repetitions); SEM, standard error mean.